# *Chapter 10*

# TRAVELING-WAVE AMPLIFIERS

The multicavity klystron amplifier described in the previous chapter was shown to have high gain and efficiency at microwave frequencies. However, its fractional bandwidth was found to be at most a few per cent. The fractional bandwidth is essentially determined by the cavity $Q$'s. Lowering these $Q$'s results in greater bandwidth, but the overall gain is reduced, as shown by Equation (9.4-17). Let us look for modifications of the multicavity-klystron-amplifier structure which will increase the bandwidth without greatly reducing the gain.

The three-cavity klystron amplifier is shown in Figure 10-1(a). The $Q$'s could be reduced by increasing the resistive loading of each cavity, either by increasing the cavity losses or by coupling each cavity to an external dissipative load. However, the power dissipated in this extra loading would be wasted. Instead, let us couple each cavity to a common transmission line, adjusting either the line length between cavities or the beam voltage so that the transmission line current arrives at the second and third cavities in phase with the current induced in these cavities by the electron beam. A suitable arrangement is shown in Figure 10-1(b). The transmission line loading has the effect of lowering the cavity $Q$'s without a corresponding power loss. The microwave power is fed forward along the transmission line, increasing the voltage in each cavity and finally appearing at the output cavity.

We can go one step further, introducing additional cavities between the three we already have, as in Figure 10-1(c). Successive cavity gaps are now closer than a quarter-plasma-wave length, so that the beam becomes only partially bunched between successive cavities. Nevertheless, the additional cavities result in a higher gain per unit length of the tube, as we shall see later, although the gain per cavity is less. As in Figure 10-1(b), the operating conditions are such that the transmission line current arrives at each

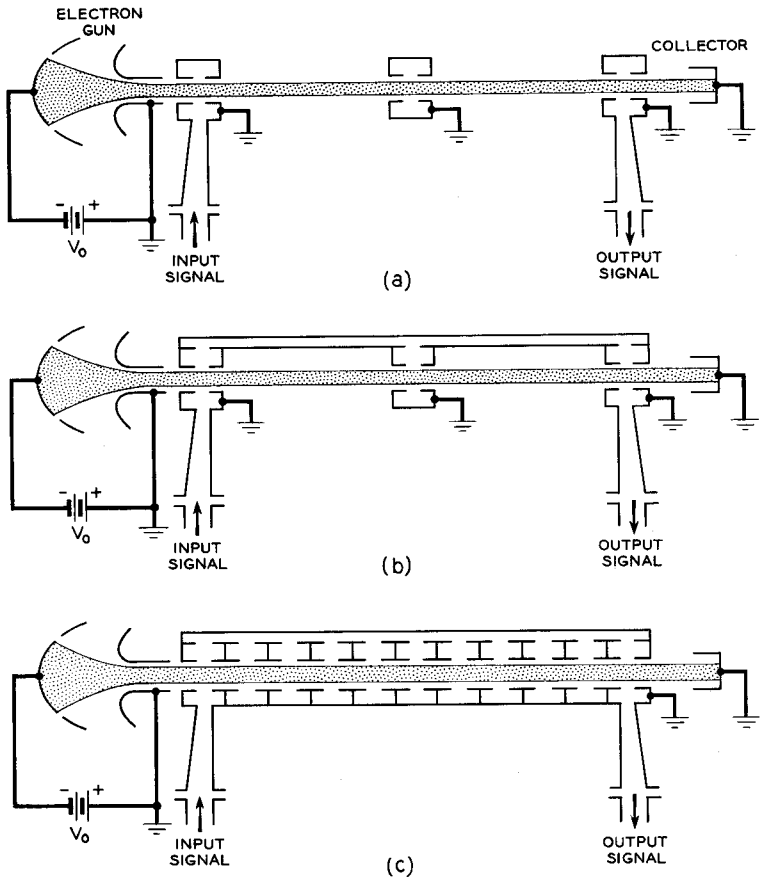


FIG. 10-1 Evolution of a traveling-wave amplifier from a multicavity klystron. (a) Multicavity klystron. (b) Multicavity klystron whose cavities are coupled by a transmission line. (c) Traveling-wave amplifier.

cavity in phase with the induced current due to the beam. The tube of Figure 10-1(c) is a traveling-wave amplifier.

One may ask: "What is the effect of the transmission line energy that travels to the left from each cavity?" In a properly designed traveling-wave amplifier, the backward-traveling energy contributions from successive cavities are of such a phase that they cancel, and thus there is no appreciable net amount of energy traveling in the backward direction.[1]

[1]In the backward-wave oscillator (Chapter 11), these backward-traveling contributions do add in phase, producing positive feedback and hence oscillations.

The assemblage of coupled cavities constitutes a slow-wave structure. As we have seen in Chapter 8, the slow-wave structure can be characterized by a Brillouin diagram, as in Figure 8.7-8. The phase shift per period of the fundamental wave on the circuit is given by

$$\theta_1 = \beta_o L \tag{10-1}$$

where $\beta_o$ is the phase shift per unit length, and $L$ is the period.

The electrons take a time $T = L/u_o$ in traveling from one cavity to another. If we wish a given electron to see *the same phase* of the rf signal as it passes through successive cavities, the phase change in a given cavity in time $T$ must be $\theta_1 + 2n\pi$. Hence

$$\omega = \frac{\theta_1 + 2n\pi}{T} = \frac{(\beta_o L + 2n\pi)u_o}{L} \tag{10-2}$$

Setting $\beta_e = \omega/u_o$, we obtain

$$\beta_e = \beta_o + \frac{2n\pi}{L} = \beta_n \tag{10-3}$$

where $\beta_n$ is the phase shift per unit length of the $n^{th}$ space harmonic Equation (10-3) may also be stated as

$$u_o = v_{pn} \tag{10-4}$$

where $v_{pn} = \omega/\beta_n$ is the space-harmonic phase velocity. Thus, traveling-wave amplification is obtained when the dc beam velocity is approximately equal to the phase velocity of the fundamental or any of the space harmonics with positive group velocity. Large fractional bandwidths are possible, since slow-wave structures may be designed with Equation (10-4) holding over a considerable frequency range.

Because of the large number of periods in practical slow-wave structures and the continuous nature of some (the helix, for example), it is convenient to treat the amplification process as the continuous interaction of velocity and convection-current waves on an electron beam with an electromagnetic wave propagating along the slow-wave circuit. This circuit wave is the space harmonic in synchronism with the beam, synchronism being defined by Equation (10-4). The nonsynchronous space harmonics have no net interaction with the electrons, and so they may be neglected. Historically, this was the approach first used in the discovery and analysis of the traveling-wave amplifier.

The interaction between an electron stream and a traveling-electromagnetic wave is illustrated in Figure 10-2, where disc electrons are used, as in Chapter 9. We view the interaction from a reference frame traveling in synchronism with the electromagnetic wave, for which the axial component of electric field is shown. In practice, the dc velocity of the electrons

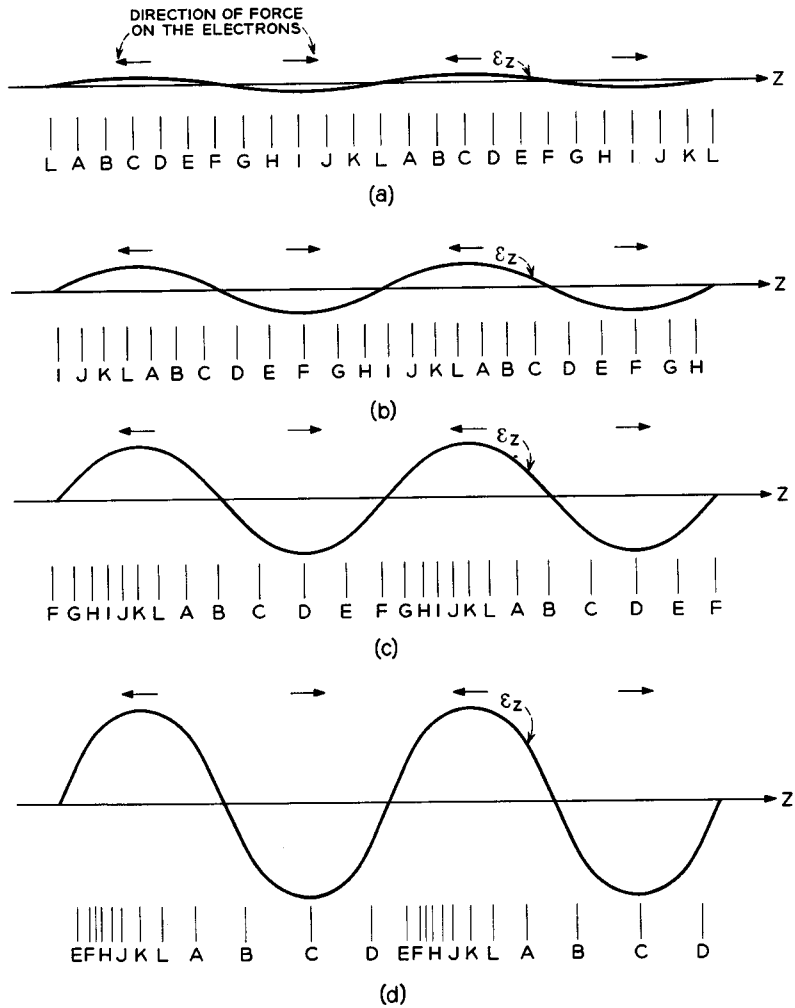


FIG. 10-2 Electron discs interacting with a traveling wave. The arrows indicate the direction of the force on the electrons due to the wave. Figure (a) corresponds to the input end of the slow-wave structure. The situations presented in Figures (b), (c), and (d) are found at positions successively farther down the tube.

is adjusted to be *slightly* greater than that of the electromagnetic wave; consequently the electrons drift to the right in the reference frame.

Figure 10-2(a) shows the conditions at the input to the slow-wave structure. The discs are uniformly spaced. Axial electric field exists due to volt-

age on the slow-wave structure from the input waveguide. This electric field exerts a force to the left on discs $A$, $B$, $C$, $D$, and $E$ and to the right on discs $G$, $H$, $I$, $J$, and $K$. These forces cause the electrons to begin to form a bunch centered about disc $L$.

Figure 10-2(b) shows the conditions farther down the tube. Since the dc velocity of the electrons is slightly greater than the wave velocity, disc $L$ has drifted into a retarding electric field, and the bunch has drifted with it. Since more electrons are in a retarding field than in an accelerating field, a net transfer of energy occurs from the beam to the electromagnetic field, thus increasing the axial electric field slightly.

In Figure 10-2(c), we observe what happens still farther down the tube. The bunch continues to become more compact and it drifts farther to the right with respect to the wave. This brings more electrons into a retarding field, and the electromagnetic wave grows in amplitude.

Figure 10-2(d) shows the conditions near the end of the tube. The bunch is even tighter, and most of the electrons are in a retarding field. An appreciable fraction of the kinetic energy of the electrons has been converted into energy stored in the electromagnetic field, and the amplitude of the field has greatly increased. The amplified wave then propagates out through the output waveguide to the load.

We note that the velocity modulation produced by the circuit electric field and the subsequent conversion to density modulation is used to transer energy from the beam to the circuit, just as in a klystron. However, unlike a klystron, velocity modulation, conversion to current modulation, and the inducing of currents into the circuit occur simultaneously and continuously along the whole length of the slow-wave structure.

In the following sections we shall consider the quantitative aspects of this interaction process.

## 10.1 Theory of the Traveling-Wave Amplifier

We shall consider the interaction process in the traveling-wave amplifier in two parts.[2] First, we shall describe the motion of the electrons which results from the rf electric fields due to both the rf circuit voltage and the rf space charge.[3] We have already considered a similar physical problem in Section 9.3, except in that case the space charge was the only source of electric field forces. The second part of this development concerns the manner in which the circuit voltage and current build up as current is induced into the circuit by the rf current in the electron beam. In the

[2]Reference 10a, Chapters 1 and 8. Reference 10b, Chapter 7.

[3]The forces due to the rf magnetic field are negligible in comparison with those due to the rf electric field.

development that follows, we shall derive two important equations, one giving the ac current induced on the beam by the rf field and one giving the rf field resulting from the modulated beam. These two equations can then be solved simultaneously to determine the self-consistent relations for the circuit and beam quantities.

We consider only the space harmonic of the circuit field in synchronism with the beam, as discussed in the introduction, since the other space harmonics travel at different phase velocities and have no cumulative interaction with the electrons.

As in the previous chapter, we consider only the rf forces, assuming that the dc forces are either zero or balanced by one of the focusing schemes described in Section 3.4. For simplicity, we assume rf motion of the electrons is possible only in the axial direction, as is the case for a strong axial magnetic field.

Script letters will be used in this section to denote time-varying quantities to distinguish them from phasor quantities.

The rf beam quantities are assumed small compared with their dc counterparts, as in Section 9.3. Under this small-signal assumption, nonlinear terms in the equations of motion can be neglected, and we obtain only linear differential equations. We shall therefore obtain wavelike solutions for the various quantities of the form

$$\mathcal{U} = \mathrm{Re}[ue^{j\omega t-\Gamma z}] \tag{10.1-1}$$

where $u$ is a phasor quantity having no time or $z$ dependence. We thus introduce a generalized phasor notation. In this notation, the phasor quantity is multiplied by

$$e^{j\omega t-\Gamma z}$$

before taking the real part. Using this notation, we have

$$\frac{\partial \mathcal{U}}{\partial t} = \mathrm{Re}[j\omega ue^{j\omega t-\Gamma z}] \tag{10.1-2}$$

and

$$\frac{\partial \mathcal{U}}{\partial z} = \mathrm{Re}[-\Gamma ue^{j\omega t-\Gamma z}] \tag{10.1-3}$$

so that partial differentiations with respect to time and $z$ correspond respectively to multiplication of the phasor quantity by $j\omega$ and $-\Gamma$. Since all the rf quantities, both circuit and beam, have variations of the form given by Equation (10.1-1), we may write the various physical equations in the phasor notation, omitting the exponential factor.

From the description of traveling-wave interaction given in the intro-

duction, we would expect $\Gamma$ to have an imaginary part approximately equal to $j\beta_e = j\omega/u_o$.

### (a) *The Electronic Equation*

The total instantaneous beam velocity, convection current, and charge density are written in the mixed phasor notation as

$$u_{\text{tot}} = u_o + u \tag{10.1-4}$$

$$i_{\text{tot}} = -I_o + i \tag{10.1-5}$$

$$\rho_{\text{tot}} = -\rho_o + \rho \tag{10.1-6}$$

where $u$, $i$, and $\rho$ are phasors representing the rf components in the notation of Equation (10.1-1).[4]

We shall assume for simplicity that the various quantities are uniform across any transverse plane of the beam. Equation (9.3-12) for the convection current density can be written as

$$i = (u_o\rho - \rho_o u)S \tag{10.1-7}$$

where $S$ is the cross-sectional area of the beam. The equation of continuity (1.3-2) is written for the phasor quantities as

$$-\Gamma i = -j\omega\rho S \tag{10.1-8}$$

Combining these two equations to eliminate $\rho$, we obtain

$$u = -\frac{j\omega - u_o\Gamma}{j\omega\rho_o S} i \tag{10.1-9}$$

relating the rf velocity and convection current.

The acceleration of an electron is given by Equation (1.1-1) as

$$\frac{d\mathfrak{u}}{dt} = -\frac{e}{m}\mathcal{E}_{zT} \tag{10.1-10}$$

where $\mathcal{E}_{zT}$ is the total instantaneous rf electric field as seen by the electron. This field is the sum of two contributions, space charge and the synchronous space harmonic due to the circuit voltage. Since the velocity of an electron is a function of both position and time, the total derivative in Equation (10.1-10) must be written as

$$\frac{d\mathfrak{u}}{dt} = \frac{\partial\mathfrak{u}}{\partial t} + \frac{\partial\mathfrak{u}}{\partial z}\frac{\partial z}{\partial t} \tag{10.1-11}$$

---

[4]The use of the symbol $i$ as a phasor quantity representing the beam convection current has become standard in microwave tube work. Unfortunately, this symbol is also used for instantaneous circuit current. The latter usage will be avoided in this and succeeding chapters on microwave tubes to avoid confusion.

For small-signal levels $\partial z/\partial t$ is approximately given by the dc beam velocity. Thus

$$\frac{d\mathfrak{u}}{dt} = \frac{\partial \mathfrak{u}}{\partial t} + u_o \frac{\partial \mathfrak{u}}{\partial z} \tag{10.1-12}$$

Equation (10.1-10) then becomes in the phasor notation:

$$\begin{aligned}(j\omega - u_o\Gamma)u &= -\frac{e}{m}E_{zT} \\ &= -\frac{e}{m}(E_{zn} + E_{zsc}) \end{aligned} \tag{10.1-13}$$

where $E_{zn}$ is the axial component of electric field contributed by the synchronous space harmonic, and $E_{zsc}$ is the field due to space charge.

In order to evaluate the field due to space charge, we merely need to solve Poisson's Equation, Equation (1.4-9), where $\rho$ is given by the rf space charge. This will be done using a one-dimensional beam of infinite cross section, with the effect of a finite beam diameter accounted for as in Section 9.3. Poisson's Equation for the one-dimensional beam is given in the phasor notation by

$$-\Gamma E_{zsc} = \frac{\rho}{\varepsilon_o} \tag{10.1-14}$$

Using Equation (10.1-8), we obtain a simple relationship between $E_{zsc}$ and the convection current:

$$E_{zsc} = j\frac{i}{\omega\varepsilon_o S} \tag{10.1-15}$$

For a finite beam, it was shown in Section 9.3 that the force due to space charge is reduced by the space-charge reduction factor $R^2$. Thus we have for a finite beam

$$E_{zsc} = jR^2\frac{i}{\omega\varepsilon_o S} \tag{10.1-16}$$

This may be written in terms of the reduced plasma frequency as

$$E_{zsc} = j\frac{m\omega_q^2}{e\rho_o S\omega}i \tag{10.1-17}$$

where use has been made of Equations (9.3-23) and (9.3-30).

Finally, Equations (10.1-9), (10.1-13), and (10.1-17) can be combined to eliminate $E_{zsc}$ and $u$. Thus we obtain

$$i = \frac{j\beta_e I_o E_{zn}}{2V_o\left[(\Gamma - j\beta_e)^2 + \dfrac{\omega_q^2}{u_o^2}\right]} \tag{10.1-18}$$

This equation is called the *electronic equation*, since it determines the ac beam convection current $i$ resulting from a given circuit voltage, as char-

acterized by the space harmonic $E_{zn}$. The time and $z$ dependence of $i$ and $E_{zn}$ are as in Equation (10.1-1).

### (*b*) *The Circuit Equation*

The convection current in the beam causes current to be induced in the circuit. This induced current adds to current already present in the circuit, causing the circuit power to increase with distance. Shortly, we shall derive an equation expressing this relationship.

It will be convenient to have a parameter that relates the space-harmonic amplitude of the electric field to the total power flow on the slow-wave circuit. Let us define the beam interaction impedance (or beam-coupling impedance) for the $n^{th}$ space harmonic as

$$K_n = \frac{\int |E_{zn}|^2 dS}{2\beta_n^2 PS} \tag{10.1-19}$$

where $|E_{zn}|$ is the amplitude of the axial electric field of the $n^{th}$ space harmonic, $\beta_n$ is the phase constant of the $n^{th}$ space harmonic, $P$ is the average circuit power flow, $S$ is the cross-sectional area of the beam, and the area integral is taken over the cross section of the beam. For brevity, we shall refer to this quantity as the impedance. We shall find later that high impedance leads to high gain per unit length of the slow-wave circuit. In order to obtain high impedance, it is important that the electric field be concentrated in the vicinity of the electron beam. This precludes the use of dielectric loaded structures, where the electric field stored in the dielectric does not contribute to the interaction with the electron beam.

As an example, we can calculate the impedance for the fundamental space harmonic of the slow-wave structure described in connection with Figure 8.7-10. The impedance is a function of the point of operation; we shall calculate it for $\beta L = \pi/4$. Assume a very thin, cylindrical beam which just grazes the top of the fingers of the structure, shown in Figure 8.7-4. Assuming that the structure is 1 cm wide, Figure 8.7-10 gives

$$P = 0.17 \text{ mw}$$

for 1 volt from one vane tip to the next, or

$$AL \sin kh = 1 \text{ volt}$$

The magnitude of the fundamental space harmonic at the tips of the vanes is obtained from Equation (8.7-37) as

$$|E_{zo}| = A \sin kh \frac{\sin \frac{\pi}{8}}{\frac{\pi}{8}} = \frac{1}{L} \frac{\sin \frac{\pi}{8}}{\frac{\pi}{8}} \text{volt}$$

$$= 0.974 \frac{1}{L} \text{volt}$$

Equation (10.1-19) for a thin beam becomes

$$K_o = \frac{|E_{zo}|^2}{2\beta_o^2 P} = \frac{(0.974)^2}{2\left(\frac{\pi}{4}\right)^2 (0.00017)}$$

$$= 4520 \text{ ohms}$$

For a thick beam the impedance would be lower, since $E_{zo}$ is strongest at the vane tips.

From Equation (10.1-19), we can define the *instantaneous power flow* along the slow-wave structure as

$$p = \frac{\mathcal{E}_{zn}^2}{\beta_n^2 K_n} \tag{10.1-20}$$

where $\mathcal{E}_{zn}$ is the instantaneous value of the space harmonic averaged over the beam cross section as in Equation (10.1-19). Differentiating this expression, we obtain

$$dp = \frac{2\mathcal{E}_{zn} d\mathcal{E}_{zn}}{\beta_n^2 K_n} \tag{10.1-21}$$

This equation expresses the change in instantaneous power flow due to an increment in the instantaneous value of the space harmonic.[5]

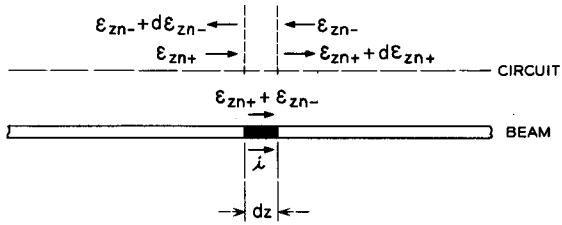


FIG. 10.1-1 Interaction of a short segment of convection current with the rf electric fields due to a slow-wave structure. The arrows above the circuit indicate directions of propagation.

Next consider Figure 10.1-1. The beam is divided up into short segments of length $dz$. Consider a typical segment in which the convection current has the instantaneous value $i$. This current segment induces currents in the circuit. These circuit currents give rise to electromagnetic waves which propagate in both directions from the point on the circuit adjacent to the

[5]For those troubled by the definition of Equation (10.1-20), an alternative derivation of Equation (10.1-21) consists of computing the instantaneous change in electric stored energy and applying Equation (8.5-26).

current segment, Let $\mathcal{E}_{zn-}$ and $\mathcal{E}_{zn+}$ be the instantaneous values of the $n^{th}$ order space harmonics moving to the left and to the right, respectively, at this point on the circuit. The induced currents due to this segment of convection current causes $\mathcal{E}_{zn-}$ to change by $d\mathcal{E}_{zn-}$ and $\mathcal{E}_{zn+}$ to change by $d\mathcal{E}_{zn+}$. Because of symmetry, we can say that

$$d\mathcal{E}_{zn-} = d\mathcal{E}_{zn+} \tag{10.1-22}$$

in other words, the incremental changes in amplitude of the waves traveling in opposite directions from the point of induction are equal.

The change in instantaneous power flow for each direction is given by Equation (10.1-21). Therefore, the total instantaneous transfer of power to the circuit is given by:

$$\begin{aligned} dp &= dp_- + dp_+ \\ &= \frac{2}{\beta_n{}^2 K_n}[\mathcal{E}_{zn-}d\mathcal{E}_{zn-} + \mathcal{E}_{zn+}d\mathcal{E}_{zn+}] \\ &= \frac{2}{\beta_n{}^2 K_n}(\mathcal{E}_{zn-} + \mathcal{E}_{zn+})d\mathcal{E}_{zn-} \\ &= \frac{2}{\beta_n{}^2 K_n}(\mathcal{E}_{zn-} + \mathcal{E}_{zn+})d\mathcal{E}_{zn+} \end{aligned} \tag{10.1-23}$$

where use has been made of Equation (10.1-22).

The incremental instantaneous power flow into the circuit from the length $dz$ of beam is given by[6]

$$dp = -i\mathcal{E}_z dz \tag{10.1-24}$$

where $i$ is the instantaneous value of the convection current, and $\mathcal{E}_z$ is the total electric field resulting from the wave on the slow-wave circuit. As discussed previously, all space harmonics are neglected, insofar as they interact with the beam, except the one in synchronism with the beam. Thus, in our case, Equation (10.1-24) becomes

$$dp = -i(\mathcal{E}_{zn-} + \mathcal{E}_{zn+})dz \tag{10.1-25}$$

for the convection current segment of Figure 10.1-1. Equations (10.1-23) and (10.1-25) can be combined to yield

$$d\mathcal{E}_{zn-} = d\mathcal{E}_{zn+} = -\tfrac{1}{2}\beta_n{}^2 K_n i dz \tag{10.1-26}$$

This may be written in the phasor notation as

$$dE_{zn-} = dE_{zn+} = -\tfrac{1}{2}\beta_n{}^2 K_n i dz \tag{10.1-27}$$

Thus, we have an expression for the incremental waves propagating away from a point on the circuit in terms of the convection current which induces them.

---

[6]This expression may be derived directly from Maxwell's Equations. See Reference 10.1.

Let $\Gamma_o = \alpha + j\beta_n$ be the complex propagation constant for the $n^{th}$ space harmonic.

Let us write an expression for the total space-harmonic field at an arbitrary point ($z = a$). This is the sum of three contributions, as follows:

A. The power coming from the input waveguide causes a field $E_{zn}(0)$ at the beginning of the circuit ($z = 0$). Thus we have at $z = a$,

$$E_{znA}(a) = E_{zn}(0)\epsilon^{-\Gamma_o a} \tag{10.1-28}$$

B. The superposition of the incremental waves $dE_{zn+}$ arriving at $z = a$ from the left is given by

$$E_{znB}(a) = \int_0^a \epsilon^{-\Gamma_o(a-z)} dE_{zn+} \tag{10.1-29}$$

C. The superposition of the incremental waves $dE_{zn-}$ arriving from the right is given by

$$E_{znC}(a) = \int_a^l \epsilon^{-\Gamma_o(z-a)} dE_{zn-} \tag{10.1-30}$$

where $l$ is the total circuit length. The total field at $z = a$ is given by the sum of these three contributions

$$E_{zn}(a) = E_{zn}(0)\epsilon^{-\Gamma_o a} - \frac{1}{2}\beta_n{}^2 K_n \int_0^a i\epsilon^{-\Gamma_o(a-z)} dz - \frac{1}{2}\beta_n{}^2 K_n \int_a^l i\epsilon^{-\Gamma_o(z-a)} dz \tag{10.1-31}$$

where use has been made of Equation (10.1-27). We can replace the variable of integration in the definite integrals by $\tau$ and we replace $a$ by $z$, an arbitrary point, obtaining

$$E_{zn}(z) = E_{zn}(0)\epsilon^{-\Gamma_o z} - \frac{1}{2}\beta_n{}^2 K_n \int_0^z i(\tau)\epsilon^{-\Gamma_o(z-\tau)} d\tau - \frac{1}{2}\beta_n{}^2 K_n \int_z^l i(\tau)\epsilon^{\Gamma_o(z-\tau)} d\tau \tag{10.1-32}$$

Thus we have an integral equation relating the field at any point to the convection current on the beam.

Equation (10.1-32) is readily converted to a differential equation by differentiation with respect to $z$. In differentiating we must be careful to handle the integrals correctly, since the limits are functions of $z$[7]. Two suc-

[7]The following formula must be used: If

$$I(z) = \int_{\alpha(z)}^{\beta(z)} F(\tau, z) d\tau$$

then

$$\frac{dI}{dx} = \int_a^\beta \frac{\partial F}{\partial z} d\tau + F(\beta, z)\frac{d\beta}{dz} - F(\alpha, z)\frac{d\alpha}{dz}$$

See Reference 10.2, p. 353, or any other book on advanced calculus.

cessive differentiations of Equation (10.1-32) yield

$$\Gamma^2 E_{zn} = \Gamma_o^2 E_{zn}(0)\epsilon^{-\Gamma_o z} - \frac{1}{2}\Gamma_o^2\beta_n^2 K_n \int_0^z i\epsilon^{-\Gamma_o(z-\tau)}d\tau$$

$$- \frac{1}{2}\Gamma_o^2\beta_n^2 K_n \int_z^l i\epsilon^{\Gamma_o(z-\tau)}d\tau + \Gamma_o\beta_n^2 K_n i \qquad (10.1\text{-}33)$$

where the left-hand side results from two successive applications of Equation (10.1-3). This result may be combined with Equation (10.1-32) yielding

$$E_{zn} = \frac{\Gamma_o\beta_n^2 K_n i}{\Gamma^2 - \Gamma_o^2} \qquad (10.1\text{-}34)$$

This equation is called the *circuit equation*, since it determines how the circuit field is affected by convection current in the beam.

### (c) *Solutions for Cumulative Interaction*

The *electronic equation* and the *circuit equation* have been derived on the assumption that the various fields and beam quantities have a $z$ dependence of the form

$$\epsilon^{-\Gamma z}$$

So far we have not said anything about values for $\Gamma$. It turns out that only certain values of $\Gamma$ are allowable when we require that the *circuit* and *electronic equations* be simultaneously satisfied.

Upon solving for the ratio $E_{zn}/i$ in both Equations (10.1-18) and (10.1-34) and equating the results, we obtain

$$(\Gamma^2 - \Gamma_o^2)\left[(\Gamma - j\beta_e)^2 + \frac{\omega_q^2}{u_o^2}\right] = \frac{j\beta_e\beta_n^2\Gamma_o K_n I_o}{2V_o} \qquad (10.1\text{-}35)$$

the solution of which determines the allowed values of $\Gamma$.

We can put this equation in a neater form by defining certain parameters.[8] First, we define the small-signal gain parameter $C$ by the equation

$$C^3 \equiv \frac{K_n I_o}{4V_o} \qquad (10.1\text{-}36)$$

$C$ is a small dimensionless parameter with values usually in the range 0.01 to 0.1.

Next, we define the space-charge parameter $QC$ by[9]

$$QC \equiv \frac{\omega_q^2}{4C^2\omega^2} \qquad (10.1\text{-}37)$$

---

[8]Reference 10a, Chapter 7.

[9]For large space charge, $QC$ is computed from the more exact expression $\sqrt{4QC^3} = \frac{\omega_q/\omega}{1 + (\omega_q/\omega)}$; see Reference 10.4.

Since $\beta_e$ and $\beta_n$ are approximately equal for synchronism, and since $\Gamma$ must have a similar imaginary part, we define the dimensionless parameters $b$, $d$, and $\delta$ by the equations

$$\Gamma_o \equiv j\beta_e(1 + Cb - jCd) \tag{10.1-38}$$

and

$$\Gamma \equiv j\beta_e(1 + jC\delta) \tag{10.1-39}$$

Since $\Gamma_o = \alpha + j\beta_n$, we see that $b$ and $d$ are real numbers given by

$$b = \frac{\beta_n - \beta_e}{\beta_e C} = \frac{u_o - v_{pn}}{v_{pn}C} \tag{10.1-40}$$

and

$$d = \frac{\alpha}{\beta_e C} \tag{10.1-41}$$

$b$ is a measure of the amount of synchronism between the electrons and the space harmonic. $d$ is directly proportional to the circuit attenuation. $\delta$ is a complex number, values of which are determined by solving Equation (10.1-35).

Equations (10.1-36) to (10.1-39) are substituted into (10.1-35). In so doing, advantage is taken of the fact that $C$ is small; that is, terms of order $C$ are neglected in comparison with terms of order unity. After simplification, we obtain

$$\delta^2 = \frac{1}{(-b + jd + j\delta)} - 4QC \tag{10.1-42}$$

where we have used the approximation

$$\frac{\Gamma_o \beta_n^2}{j\beta_e^3} \cong 1 \tag{10.1-43}$$

Equation (10.1-42) is a cubic equation in the unknown $\delta$. The solutions, when introduced into Equation (10.1-39), give us three allowable values for $\Gamma$, the complex propagation constant for the circuit-beam coupled system.[10] From Equation (10.1-42), we note that the solutions are functions of $b$ (the degree of synchronism), $d$ (the circuit attenuation), and $QC$ (the space charge).

From Equation (10.1-39), we note that the difference between $\Gamma$ and $j\beta_e$ is directly proportional to $C$, which from Equation (10.1-36) is a function of

[10]Since Equation (10.1-35) is a quartic equation, we see that one root has been lost due to the approximations we have made. This root corresponds to a backward propagating wave, which is nonsynchronous with the beam and which is not excited for proper termination of the circuit.

the amount of coupling between the beam and the circuit. The stronger the coupling (the larger $K_n$ is), the greater is this difference, as we should expect for two coupled systems.

Let us examine the nature of the solutions for the simple case:

$$b = d = QC = 0$$

Equation (10.1-42) reduces to

$$\delta^3 = -j \tag{10.1-44}$$

with solutions

$$\begin{aligned} \delta_1 &= \frac{\sqrt{3}}{2} - j\frac{1}{2} \\ \delta_2 &= -\frac{\sqrt{3}}{2} - j\frac{1}{2} \\ \delta_3 &= j \end{aligned} \tag{10.1-45}$$

The values of $\Gamma$ are then given by

$$\begin{aligned} \Gamma_1 &= -\frac{\sqrt{3}}{2}\beta_e C + j\beta_e\left(1 + \frac{C}{2}\right) \\ \Gamma_2 &= \frac{\sqrt{3}}{2}\beta_e C + j\beta_e\left(1 + \frac{C}{2}\right) \\ \Gamma_3 &= j\beta_e(1 - C) \end{aligned} \tag{10.1-46}$$

Since the various fields and beam quantities propagate as

$$\epsilon^{j\omega t - \Gamma z}$$

we see that $\Gamma_1$ corresponds to a traveling wave whose amplitude grows exponentially with distance, $\Gamma_2$ to one whose amplitude decays exponentially with distance, and $\Gamma_3$ to a wave of constant amplitude. The wave corresponding to $\Gamma_1$ is termed the *growing wave*, and it is this wave which is responsible for the gain in the traveling-wave tube. We shall find that, regardless of the values of $d$ and $QC$, we shall always obtain one growing wave, one decaying wave, and one wave of nearly constant amplitude, as long as $b$ corresponds to operation sufficiently close to synchronism.[11]

We can examine the condition of synchronism for this example. It was pointed out in connection with Figure 10-2 that the electrons must travel slightly faster than the wave so that the bunch drifts into a retarding field. It is clear that the growing wave will predominate as the electrons move down the tube. Thus, the circuit field depicted in Figure 10-2 near the end

[11] $d$, of course, must not be so large as to neutralize the gain of the growing wave.

of the tube has $\Gamma_1$ for its propagation constant, corresponding to a phase velocity given by

$$v_{p1} = \frac{\omega}{\beta_e(1 + \frac{1}{2}C)} = \frac{u_o}{1 + \frac{1}{2}C} \tag{10.1-47}$$

which is indeed slightly slower than the dc beam velocity. Thus, although the cold (no electrons) phase velocity $v_{pn}$ is exactly equal to $u_o$ from Equation (10.1-40), the hot phase velocity of the growing wave $v_{p1}$ is slower than $u_o$. This must be true regardless of the values of $b$, $d$, and $QC$ if we are to obtain amplification.

As a second example, we consider the condition of large space charge. Let the circuit attenuation be zero ($d = 0$), for simplicity. Under the condition that $QC$ is large, we may neglect the first term on the right-hand side of Equation (10.1-42) in comparison with the second term, obtaining

$$\delta^2 \cong -4QC \tag{10.1-48}$$

with the solutions

$$\delta_1,\delta_3, \cong \pm j2\sqrt{QC} \tag{10.1-49}$$

From Equation (10.1-39), we obtain

$$\begin{aligned}\Gamma_1,\Gamma_3 &\cong j\beta_e(1 \pm 2C\sqrt{QC}) \\ &\cong j\beta_e\left(1 \pm \frac{\omega_q}{\omega}\right)\end{aligned} \tag{10.1-50}$$

for the growing wave and constant-amplitude wave, respectively. Referring back to Equations (9.3-40) and (9.3-41), we see that these propagation constants correspond to the slow and fast space-charge waves, respectively. The approximate form of Equation (10.1-48) does not allow computation of the real parts associated with these waves. Furthermore, the decaying wave propagation constant $\Gamma_2$ is not evaluated at all. Numerical calculations can be used to derive this information directly from Equation (10.1-42).[12] The result of such a calculation is given in Figure 10.1-2, for $QC = 1$. The real and imaginary parts of $\delta$ are defined by

$$\delta = x + jy \tag{10.1-51}$$

We note from this figure that a growing wave (positive values of $x$) is obtained for $b$ approximately between 0.9 and 2.8, with a maximum value of $x_1$ equal to 0.5. The value of $b$ corresponding to this maximum value of $x_1$ determines the electron velocity for maximum gain. A useful approximate formula for the maximum value of $x_1$ as a function of $QC$ is[13]

$$x_{1\,\max} \cong \frac{1}{2(QC)^{1/4}} \tag{10.1-52}$$

---

[12]Reference 10a, Chapter 8.
[13]Reference 10.3.

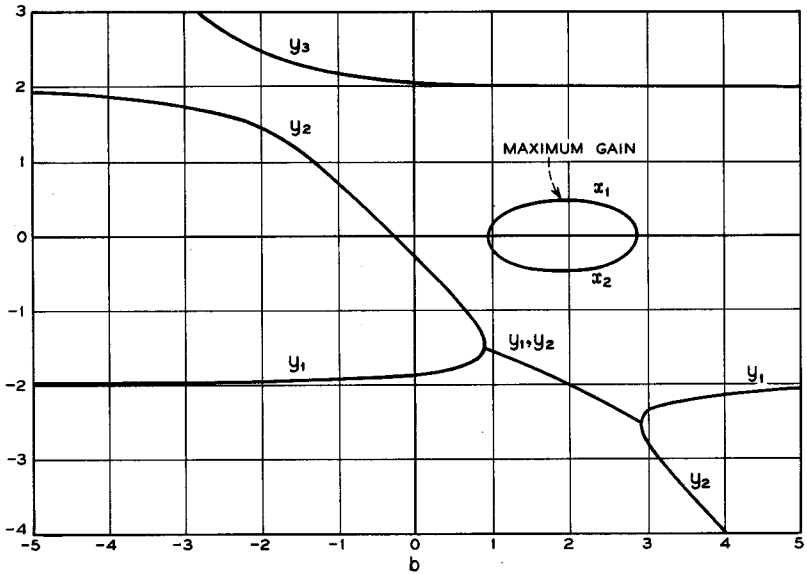


FIG. 10.1-2 Real and imaginary parts of the three solutions for $\delta$ for a traveling-wave amplifier with zero loss and $QC = 1$. (From John R. Pierce, *Traveling Wave Tubes*, D. Van Nostrand Co., Inc., Princeton, N. J., 1950)

Having determined the three allowed values of the propagation constant $\Gamma$, which correspond to waves propagating in the forward direction, one can write an expression for the rf components of the total electric field, the velocity, and the convection current as

$$\begin{aligned} E_{zT} &= E_{zT1}\epsilon^{-\Gamma_1 z} + E_{zT2}\epsilon^{-\Gamma_2 z} + E_{zT3}\epsilon^{-\Gamma_3 z} \\ u &= u_1\epsilon^{-\Gamma_1 z} + u_2\epsilon^{-\Gamma_2 z} + u_3\epsilon^{-\Gamma_3 z} \\ i &= i_1\epsilon^{-\Gamma_1 z} + i_2\epsilon^{-\Gamma_2 z} + i_3\epsilon^{-\Gamma_3 z} \end{aligned} \tag{10.1-53}$$

The values of the component waves can be found from the initial conditions at $z = 0$, the input end of the slow-wave circuit. Since the beam is unmodulated at this point, we have

$$\begin{aligned} u(0) &= 0 \\ i(0) &= 0 \end{aligned} \tag{10.1-54}$$

For the same reason, the rf space-charge field is zero and the total electric field is given by the circuit voltage alone,

$$E_{zT}(0) = E_{zn}(0) \tag{10.1-55}$$

The latter quantity may be determined in magnitude from the rf input power using Equation (10.1-19), which can be written as

$$| E_{zn} |^2 = 2\beta_n^2 K_n P \tag{10.1-56}$$

where $| E_{zn} |$ is the rms average over the beam cross section. We assume all the quantities $u$, $i$, etc., are similar rms averages.

Before applying the above boundary conditions, we derive certain other relationships between $E_{zT}$, $u$, and $i$. First, we introduce Equation (10.1-39) into (10.1-13), obtaining

$$u_\nu = -\frac{e}{m\omega C\delta_\nu} E_{zT\nu} \tag{10.1-57}$$

for $\nu = 1,2,3$, that is, for each of the three waves. Next, we introduce Equation (10.1-39) into (10.1-9), obtaining

$$i_\nu = -\frac{j\rho_o S}{C\delta_\nu} u_\nu \tag{10.1-58}$$

which with Equation (10.1-57) becomes

$$i_\nu = \frac{je\rho_o S}{m\omega C^2\delta_\nu^2} E_{zT\nu} \tag{10.1-59}$$

Equations (10.1-57) and (10.1-59) may be substituted into Equations (10.1-53) so that the total electric field is the only variable. When this is done, and the boundary conditions (10.1-54) and (10.1-55) are applied, Equations (10.1-53) become

$$\begin{aligned} E_{zn}(0) &= E_{zT1} + E_{zT2} + E_{zT3} \\ 0 &= \frac{1}{\delta_1} E_{zT1} + \frac{1}{\delta_2} E_{zT2} + \frac{1}{\delta_3} E_{zT3} \\ 0 &= \frac{1}{\delta_1^2} E_{zT1} + \frac{1}{\delta_2^2} E_{zT2} + \frac{1}{\delta_3^2} E_{zT3} \end{aligned} \tag{10.1-60}$$

Since the $\delta$'s are known, these three simultaneous equations may be solved to obtain solutions for $E_{zT1}$, $E_{zT2}$, and $E_{zT3}$ in terms of $E_{zn}(0)$. The solution for the growing wave is given by

$$\frac{E_{zT1}}{E_{zn}(0)} = \frac{\delta_1^2}{(\delta_1 - \delta_2)(\delta_1 - \delta_3)} \tag{10.1-61}$$

We define the initial loss factor $A_1$ in decibels by the expression

$$A_1 = 20 \log \left| \frac{E_{zT1}}{E_{zn}(0)} \right| \text{db} \tag{10.1-62}$$

which can be evaluated from Equation (10.1-61).

The total power gain of the traveling-wave amplifier may be written as

$$\text{gain} = 20 \log \left| \frac{E_{zn}(l)}{E_{zn}(0)} \right| \text{db} \tag{10.1-63}$$

where $l$ denotes the output end of the slow-wave structure. For a practical tube where the gain is 20 db or more, the fields at the output end of the structure are given very accurately by the growing wave alone, so we may write

$$\text{gain} = 20 \log \left| \frac{E_{zn1}\epsilon^{-\Gamma_1 l}}{E_{zn}(0)} \right| \text{db} \tag{10.1-64}$$

This can be written as

$$\text{gain} = 20 \log \left| \frac{E_{zT1}}{E_{zn}(0)} \frac{E_{zn1}}{E_{zT1}} \epsilon^{-\Gamma_1 l} \right| \text{db} \tag{10.1-65}$$

Since

$$| \epsilon^{-\Gamma_1 l} | = \epsilon^{\beta_e C x_1 l} \tag{10.1-66}$$

Equation (10.1-65) becomes

$$\text{gain}_{db} = A_1 + 20\beta_e C x_1 l \log \epsilon + A_2 \tag{10.1-67}$$

where

$$A_2 = 20 \log \left| \frac{E_{zn1}}{E_{zT1}} \right| \text{db} \tag{10.1-68}$$

The quantity $A_2$ is termed the space-charge loss factor, since it is a measure of the ratio of the circuit field $E_{zn}$ to the total field, at the end of the circuit where the growing wave predominates. We further define

$$B = (40\pi \log \epsilon) x_1 = 54.6 x_1 \tag{10.1-69}$$

and the number of electronic wavelengths on the circuit $N$ by

$$N = \frac{\beta_e l}{2\pi} \tag{10.1-70}$$

so that Equation (10.1-67) for the gain of a traveling-wave amplifier becomes

$$\text{gain}_{db} = A_1 + A_2 + BCN \tag{10.1-71}$$

Finally, we must evaluate $A_2$, the space-charge loss factor. Equation (10.1-59) may be written for the growing wave as

$$i_1 = \frac{j e \rho_0 S}{m\omega C^2 \delta_1^2} E_{zT1} \tag{10.1-72}$$

This equation is combined with Equation (10.1-17) written for the growing wave to eliminate $i_1$. After simplifying and introducing the definition of $QC$, Equation (10.1-37), one obtains

$$\frac{E_{zn1}}{E_{zT1}} = \frac{\delta_1^2 + 4QC}{\delta_1^2} \tag{10.1-73}$$

recalling that $E_{zT1} = E_{zn1} + E_{zsc1}$. From Equation (10.1-68), $A_2$ is thus given by

$$A_2 = 20 \log \left| \frac{\delta_1^2 + 4QC}{\delta_1^2} \right| \text{db} \tag{10.1-74}$$

In conclusion, we write an expression for the gain when $b = d = QC = 0$. From Equations (10.1-45), we calculate

$$A_1 = -9.54 \text{ db}$$
$$A_2 = 0 \text{ db}$$
$$B = 47.3$$

so that Equation (10.1-71) becomes

$$\text{gain}_{db} = -9.54 + 47.3CN \tag{10.1-75}$$

*(d) Summary of Gain Calculation*

Let us review the steps in calculating the gain of a traveling-wave amplifier. Knowing the properties of the beam and the circuit, we calculate $C$, $N$, $b$, $d$, and $QC$ as follows:

$$C = \left[ \frac{K_n I_o}{4V_o} \right]^{1/3} \tag{10.1-36}$$

$$N = \frac{\beta_e l}{2\pi} = \frac{u_e l}{2\pi\omega} \tag{10.1-70}$$

$$b = \frac{\beta_n - \beta_e}{\beta_e C} \tag{10.1-40}$$

$$d = \frac{\alpha}{\beta_e C} \tag{10.1-41}$$

$$QC = \frac{\omega_q^2}{4C^2\omega^2} \tag{10.1-37}$$

$K_n$ is defined as in Equation (10.1-19) $\delta_1$, $\delta_2$, and $\delta_3$ are determined as the three roots of the cubic equation:

$$\delta^2 = \frac{1}{(-b + jd + j\delta)} - 4QC \tag{10.1-42}$$

Next, $A_1$ and $A_2$ are calculated from the equations:

$$A_1 = 20 \log \left| \frac{\delta_1^2}{(\delta_1 - \delta_2)(\delta_1 - \delta_3)} \right| \text{db} \tag{10.1-62}$$

and

$$A_2 = 20 \log \left| \frac{\delta_1^2 + 4QC}{\delta_1^2} \right| \text{db} \tag{10.1-74}$$

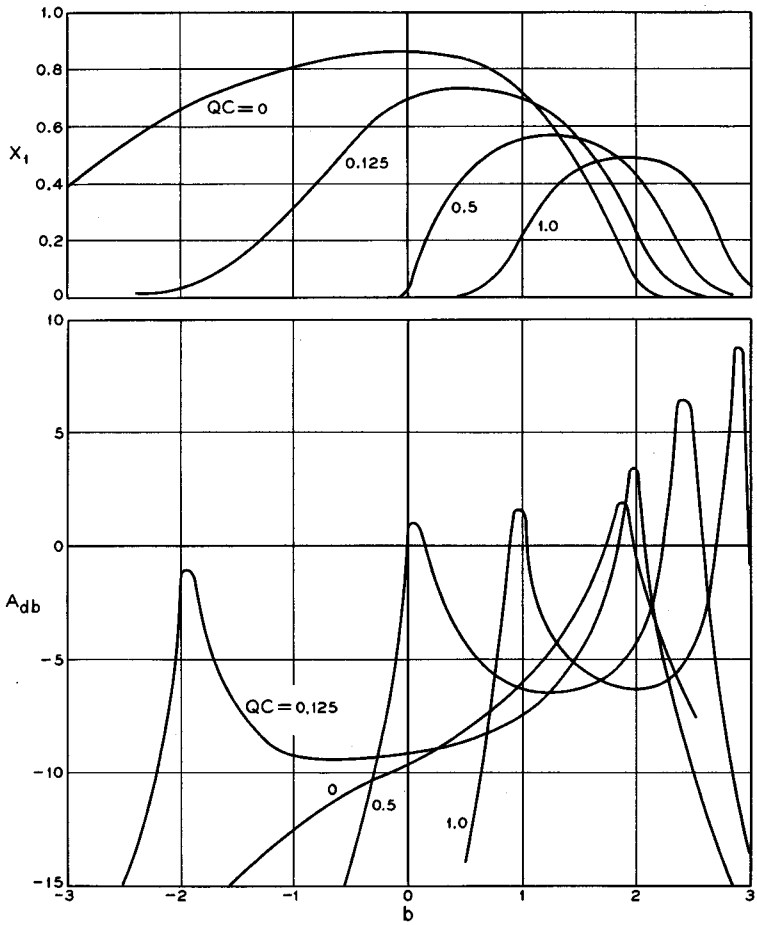


FIG. 10.1-3 Graphs useful in calculating the gain of a traveling-wave amplifier. $d = 0.025$. $C = 0$. Curves for non-zero values of $C$ are given in Reference 10.4. (Courtesy of *Transactions IRE*)

Finally, the gain is computed from the equation:

$$\text{gain}_{db} = A_1 + A_2 + BCN \tag{10.1-71}$$

where

$$B = 54.6x_1 \tag{10.1-69}$$

Considerable effort can be saved by using charts which give $x_1$ and $A = A_1 + A_2$ directly in terms of $b$, $d$, and $QC$.[14] Such a chart is shown in Figure 10.1-3, where $x_1$ and $A$ are plotted vs. $b$ for $d = 0.025$ and various values of $QC$. By these methods one can calculate the gain of a traveling-wave amplifier and the variation with frequency.

## 10.2 High-Power Tubes

The theory developed in the previous section enables one to calculate the performance of a traveling-wave amplifier once the properties of the beam and the slow-wave structure are known. We must know two things about the slow-wave structure — the Brillouin diagram and the strength of coupling to the electron beam. The latter quantity is measured in terms of the

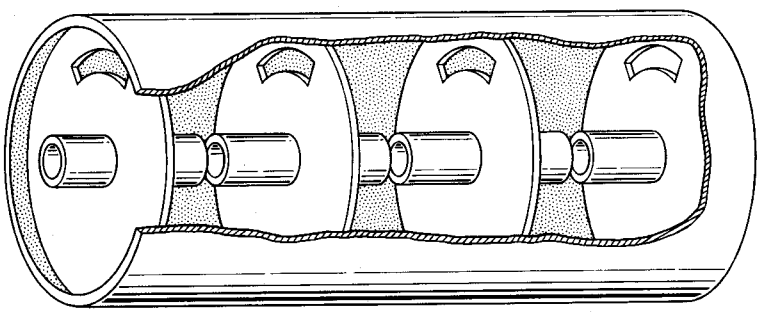

FIG. 10.2-1 High-power slow-wave structure consisting of a cascade of re-entrant cavity resonators, with mutual inductive coupling obtained through apertures in their common walls.

beam-coupling impedance $K_n$. In this section we examine some of the techniques used to evaluate these quantities for a typical high-power structure.

### (a) *The Brillouin Diagram*

The slow-wave structure of Figure 10-1(c) is well suited for high-power interaction. The large metal surfaces in this structure serve the dual pur-

[14]Reference 10.4. Curves for $C = 0.2$ are in error. Corrected curves are given in Reference 10.5, Figure 4(c).

pose of keeping rf ohmic losses small and also of providing means for removing the heat due to beam interception on the re-entrant parts of the cavities. A simplified version of this structure is presented in Figure 10.2-1. In this structure, the coupling between cavities is obtained by means of coupling apertures placed in the inductive portions of the cavities. These apertures allow portions of the magnetic flux of one cavity to link the adjacent cavities, so as to provide mutual coupling between cavities.

An equivalent circuit for this structure is shown in Figure 10.2-2. $L_1$ and $C_1$ are the inductance and capacitance of each re-entrant cavity, as dis-

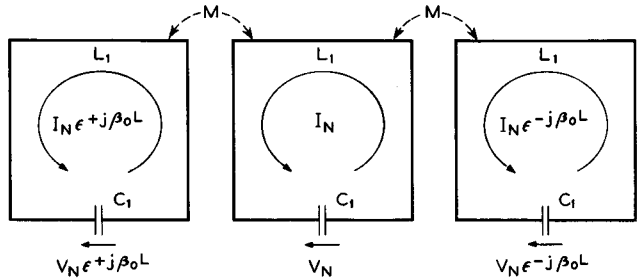


FIG. 10.2-2 Equivalent circuit for the slow-wave structure of Figure 10.2-1.

discussed in Chapter 8. The inductance is shown as a single turn. $M$ is the mutual inductance between cavities; obviously it becomes larger as one increases the size of the coupling aperture. Loop currents are shown in each of the cavities. From Floquet's Theorem we know that, if the current in the $N^{th}$ cavity is $I_N$, the currents in the $N-1$ and $N+1$ cavities are given by

$$I_N\epsilon^{+j\beta_0 L}$$

and

$$I_N\epsilon^{-j\beta_0 L}$$

respectively.

From Kirchhoff's voltage law, we can write the loop equation for the $N^{th}$ loop as

$$\left(j\omega L_1 + \frac{1}{j\omega C_1}\right)I_N - j\omega M I_N\epsilon^{j\beta_0 L} - j\omega M I_N\epsilon^{-j\beta_0 L} = 0 \qquad (10.2\text{-}1)$$

This may be simplified to yield

$$\cos\beta_0 L = \frac{1}{k_1}\left(1 - \frac{\omega_c^2}{\omega^2}\right) \qquad (10.2\text{-}2)$$

where $k_1 = 2M/L_1$ is the coupling coefficient, and $\omega_c = 1/\sqrt{L_1C_1}$ is the

radian resonant frequency of the cavity. The upper and lower cutoff frequencies are obtained from Equation (10.2-2) as

$$\omega_2 = \frac{\omega_c}{\sqrt{1 - k_1}} \quad \text{at} \quad \beta_o L = 0$$

and

$$\omega_1 = \frac{\omega_c}{\sqrt{1 + k_1}} \quad \text{at} \quad \beta_o L = \pi \tag{10.2-3}$$

For $k_1 = 0$, the Brillouin diagram is a horizontal line given by $\omega = \omega_c$. Increasing the coupling increases the width of the passband.

The Brillouin diagram is shown in Figure 10.2-3 for the fundamental and $-1$ space harmonics for a value of $k_1$ equal to 0.4, as obtained from Equation (10.2-2). The fundamental is a backward wave, since its group and

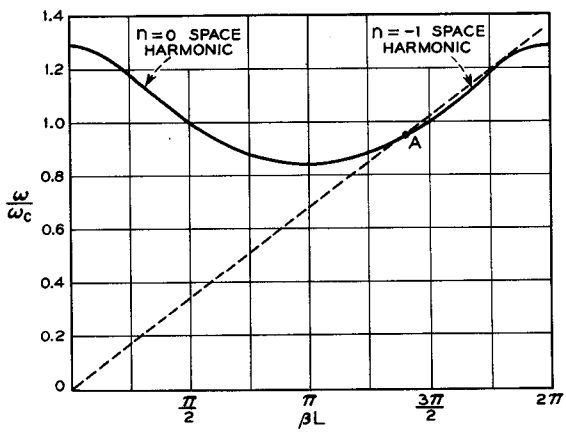


FIG. 10.2-3 Brillouin diagram for the slow-wave structure of Figure 10.2-1, for $k_1 = 0.4$. A voltage line is shown corresponding to typical interaction with the $-1$ space harmonic for forward wave interaction.

phase velocities are in opposite directions. In the traveling-wave amplifier a forward wave is necessary for amplification, since the power on the circuit travels in the same direction as the electron beam. The $-1$ space harmonic is such a wave. The slope of the line joining the origin to point $A$ gives the phase velocity of the space harmonic at the point $A$. Since this line is nearly tangent to the $-1$ space-harmonic curve, the phase velocity is nearly constant over a moderately wide frequency range. Thus, with the dc beam velocity equal to this phase velocity, synchronous interaction is obtainable over a considerable frequency range.

### (b) *The Beam Interaction Impedance*

In calculating the beam interaction impedance, we shall need an expression for the total power flow in the circuit. This could be obtained directly from the equivalent circuit using network theory. However, it is easier to obtain the power from the group velocity and the average stored energy per period, as in Section 8.7(d). The average stored energy is equal to the peak electric stored energy,

$$W_L = \tfrac{1}{2}C_1 \mid V_N \mid^2 \tag{10.2-4}$$

where $V_N$ is the voltage across the $N^{\text{th}}$ gap. The group velocity of the fundamental is obtained by means of a differentiation of Equation (10.2-2) as

$$v_g = \frac{d\omega}{d\beta_o} = -\frac{k_1 L}{2}\frac{\omega^3}{\omega_c^2}\sin \beta_o L \tag{10.2-5}$$

All the space harmonics have the same magnitude of group velocity at the same frequency. From Equation (8.7-49) the power flow in the forward direction is thus given by

$$P = \frac{k_1 \omega^3 C_1}{4\omega_c^2} \mid V_N \mid^2 \sin \beta_o L \tag{10.2-6}$$

In order to evaluate the impedance by Equation (10.1-19) we need an expression for the amplitude of the space harmonic. This is obtained by solving Maxwell's Equations in the region of the beam.

Consider Figure 10.2-4. A series of concentric cylinders of inside radii $a$ uniformly spaced along the $z$ axis is shown. The periodic spacing is $L$, and the gap between cylinders is $\delta$. The voltage across gap $N$ is $V_N$, and we assume that the electric field across the gap at $r = a$ is uniform and equal to $V_N/\delta$.

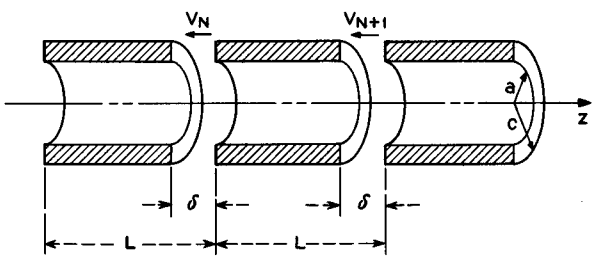


FIG. 10.2-4 Identical, concentric cylinders uniformly spaced along the $z$ axis. The gap voltages obey Floquet's Theorem. The internal fields are analyzed in terms of space harmonics.

We confine our attention to the region $r \leq a$. The general solution for the electric field in this region is given by Equation (8.7-16), for which the $z$ component is

$$E_z(x,y,z) = \sum_{-\infty}^{\infty} E_{zn}(x,y)\epsilon^{-j\beta_n z} \tag{10.2-7}$$

As shown in Section 8.7, each space harmonic will by itself satisfy the wave Equation (8.1-26). The $z$ component of the wave equation for the $n^{\text{th}}$ space harmonic can be written as

$$\left(\frac{\partial^2}{\partial x^2} + \frac{\partial^2}{\partial y^2}\right)E_{zn} - (\beta_n{}^2 - k^2)E_{zn} = 0 \tag{10.2-8}$$

similar to Equation (8.7-27). Since the structure in Figure 10.2-4 has cylindrical symmetry about the $z$ axis, it will be more convenient to write the above equation in cylindrical coordinates. The two-dimensional Laplacian can be written as

$$\frac{\partial^2}{\partial x^2} + \frac{\partial^2}{\partial y^2} = \frac{\partial^2}{\partial r^2} + \frac{1}{r}\frac{\partial}{\partial r} + \frac{1}{r^2}\frac{\partial^2}{\partial \theta^2} \tag{10.2-9}$$

in polar coordinates.[15] Since the boundary conditions in Figure 10.2-4 have no functional dependence on $\theta$, we look for space harmonics which also are independent of $\theta$. The last term in Equation (10.2-9) is thus set equal to zero. Equation (10.2-8) becomes

$$\left[\frac{\partial^2}{\partial r^2} + \frac{1}{r}\frac{\partial}{\partial r} - \gamma_n{}^2\right]E_{zn} = 0 \tag{10.2-10}$$

where $\gamma_n{}^2 = \beta_n{}^2 - k^2$ and is positive for slow waves. $k$ is equal to $\omega/c$.

Equations (10.2-10) may be written in a form recognizable as Bessel's Equation,

$$\left[\frac{\partial^2}{\partial r^2} + \frac{1}{r}\frac{\partial}{\partial r} + \tau_n{}^2\right]E_{zn} = 0 \tag{10.2-11}$$

with $\tau_n{}^2 = -\gamma_n{}^2$. The solution of this equation is well known:

$$E_{zn} = B_n J_o(\tau_n r) \tag{10.2-12}$$

where $J_o$ is the Bessel function of the first kind of order 0, and $B_n$ is an arbitrary constant. Thus, the solution of Equation (10.2-10) is given by

$$E_{zn} = B_n J_o(j\gamma_n r) \tag{10.2-13}$$

This modified Bessel function has a real value despite the fact that the

---

[15]Reference 10.2, p. 328. This may also be derived using the relations of Appendix XII together with the definition of the Laplacian of a scalar, $\nabla^2\Phi = \nabla \cdot \nabla\Phi$.

argument is a pure imaginary quantity. This function is of sufficient importance that it is given its own symbol,

$$J_o(j\gamma_n r) \equiv I_o(\gamma_n r) \tag{10.2-14}$$

It is plotted in Figure 10.2-5. From this figure we see that the axial electric field is weakest on the axis and strongest at the circuit. This behavior was also obtained in the slow-wave structure of Figure 8.7-4. In fact, this is a

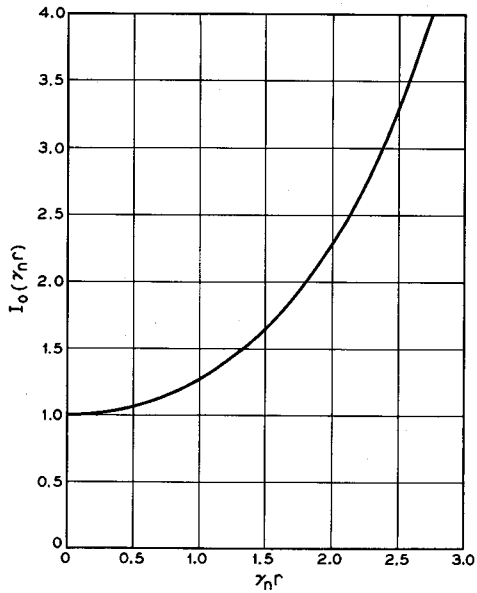


FIG. 10.2-5 Modified Bessel function which gives the radial decay of the axial component of a cylindrically symmetric space harmonic.

general characteristic of slow-wave structures; the axial field is strongest at the circuit. Most traveling-wave amplifiers have a value of $\gamma_n r$ at the circuit in the range of 1 to 2 for the synchronous space harmonic. Thus, the field on the axis may be only half that at the circuit.

Equation (10.2-7) may thus be written as

$$E_z(r,z) = \sum_{-\infty}^{\infty} B_n I_o(\gamma_n r) \epsilon^{-j\beta_n z} \tag{10.2-15}$$

The space-harmonic amplitudes $B_n$ are evaluated by imposing the boundary conditions at $r = a$. We take $z = 0$ to correspond to the center of the $N^{\text{th}}$ gap. If we confine our attention to the unit cell centered at $z = 0$, we have

from Equation (10.2-15):

$$\sum_{-\infty}^{\infty} B_n I_o(\gamma_n a)\epsilon^{-j\beta_n z} = \begin{cases} \frac{V_N}{\delta} \text{ for } |z| < \frac{\delta}{2} \\ 0 \text{ for } \frac{\delta}{2} < |z| < \frac{L}{2} \end{cases} \tag{10.2-16}$$

Multiplying both sides of this equation by $\epsilon^{+j\beta_m z}$ and integrating over the range $|z| \leq L/2$, we obtain

$$B_m L I_o(\gamma_m a) = \frac{V_N}{\delta} \frac{\sin \beta_m \frac{\delta}{2}}{\frac{\beta_m}{2}} \tag{10.2-17}$$

where use has been made of Equation (8.7-35). The axial electric field is thus given by the expression

$$E_z(r,z) = \frac{V_N}{L} \sum_{-\infty}^{\infty} \frac{\sin \beta_n \frac{\delta}{2}}{\beta_n \frac{\delta}{2}} \frac{I_o(\gamma_n r)}{I_o(\gamma_n a)} \epsilon^{-j\beta_n z} \tag{10.2-18}$$

The impedance for the $n^{\text{th}}$ space harmonic is obtained by introducing Equation (10.2-6) into Equation (10.1-19) together with the space-harmonic amplitude obtained from Equation (10.2-18). One obtains

$$K_n = M_{1(n)}{}^2 M_{2(n)}{}^2 \frac{2\omega_c{}^2}{(\beta_n L)^2 k_1 \omega^3 C_1 \sin \beta_o L} \tag{10.2-19}$$

where

$$M_{1(n)} = \frac{\sin \beta_n \frac{\delta}{2}}{\beta_n \frac{\delta}{2}} \tag{10.2-20}$$

is the gap factor for the $n^{\text{th}}$ space harmonic, and

$$M_{2(n)}{}^2 = \frac{1}{S I_o{}^2(\gamma_n a)} \int I_o{}^2(\gamma_n r) dS \tag{10.2-21}$$

is the impedance reduction factor obtained by integrating the radial variation of the electric field over the cross section of the beam. Both factors are less than or equal to unity.

The impedance for the $-1$ space harmonic plotted in Figure 10.2-3 is obtained from Equation (10.2-19) by setting $n$ equal to $-1$. The result is plotted in Figure 10.2-6 for $k_1$ and $\delta/L$ both equal to 0.4. The impedance

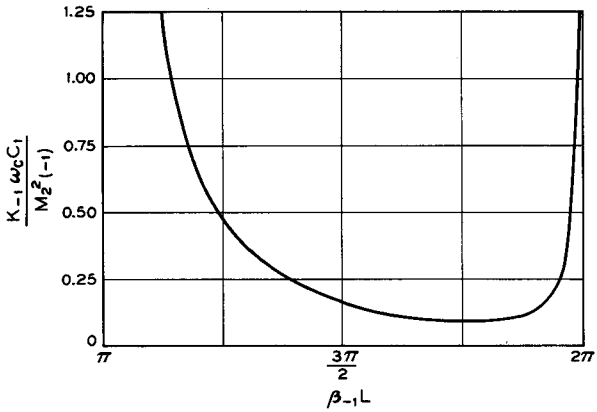


FIG. 10.2-6 Normalized impedance for the $-1$ space harmonic of the slow-wave structure of Figure 10.2-1. $k_1 = \delta/L = 0.4$.

is seen to become infinite at both band edges since the group velocity goes to zero at these frequencies.

### (c) *A Numerical Example*

As an example we calculate $K_{-1}$ at band center for a typical circuit. Assume that the cylinders shown in Figure 10.2-4 have the following dimensions:

$$a = 2 \text{ mm}$$
$$c = 2.5 \text{ mm}$$
$$\delta = 2 \text{ mm}$$
$$L = 5 \text{ mm}$$

The structure is designed for a center frequency of 6000 Mc with $k_1 = 0.4$. Assume an electron beam of very small diameter on the axis; under this condition,

$$M_{2(-1)}^2 = \frac{1}{I_o^2(\gamma_{-1}a)}$$

Using the relation $\gamma_{-1}^2 = \beta_{-1}^2 - k^2$, we obtain

$$\gamma_{-1}a = 0.992\beta_{-1}a = 0.992\frac{a}{L}\beta_{-1}L = 0.992(0.4)\frac{3\pi}{2} = 1.87$$

From Figure 10.2-5,

$$M_{2(-1)}^2 = \frac{1}{I_o^2(1.87)} = 0.230$$

In calculating the capacitance between cylinders we must make an allowance for fringing effects. It has been found empirically that the capacitance is about four times that given by the simple parallel plate formula for the dimensions given. Thus,

$$C_1 \cong 4\frac{\varepsilon_0 2\pi a(c-a)}{\delta} \cong 0.111 \text{ pf}$$

The ordinate in Figure 10.2-6 is read as 0.1635 at band center. Thus,

$$K_{-1} = 0.1635\frac{M_{2(-1)}^2}{\omega_c C_1} = 0.1635\frac{0.230}{(12\pi 10^9)(0.111 \times 10^{-12})} = 9.0 \text{ ohms}$$

This value of impedance is typical of circuits of this type.

With the above information it is necessary only to specify the beam current and structure length to complete the description of the amplifier. The beam voltage is determined by the synchronism condition, $\beta_e = \beta_{-1}$, at some frequency within the band.

Operation as a forward-wave amplifier is also possible in higher-order space harmonics, such as the $-2$, $-3$, $-4$, etc. However, from Equation (10.2-19), it is seen that the impedance falls off for these higher-space harmonics, because $\beta_n L$ is larger and $M_{1(n)}$ and $M_{2(n)}$ are smaller. Therefore, the lowest possible order forward space harmonic is always used so as to obtain maximum interaction. This explains why the structure of Figure 10-1(c) is superior to that of Figure 10-1(b); for the same voltage, the latter corresponds to higher space-harmonic interaction, under the usual condition $\omega_q/\omega \ll 1$.

### (*d*) *Description of a Practical Power Traveling-Wave Tube*

Figure 10.2-7 shows the construction of the Bell Telephone Laboratories type M4040 traveling-wave amplifier.[16] A photograph of the tube is shown in Figure 10.2-8. This tube was designed to be the ground transmitter tube in the *Telstar* experimental satellite communications system. It uses a slow-wave structure similar to the one in Figure 10.2-1, except that the inductive coupling holes appear alternately at the top and bottom of the discs separating the cavities. This is done primarily to prevent inductive coupling between cavities which are not directly adjacent.

The slow-wave structure actually consists of two separate sections, nearly equal in length, placed end to end. Each section has its own rf input and output connections. The input rf signal is introduced onto the first section close to the electron gun. This signal is amplified by 17 db and then coupled out into an external sever termination. The electron bunches

[16]Reference 10.6.

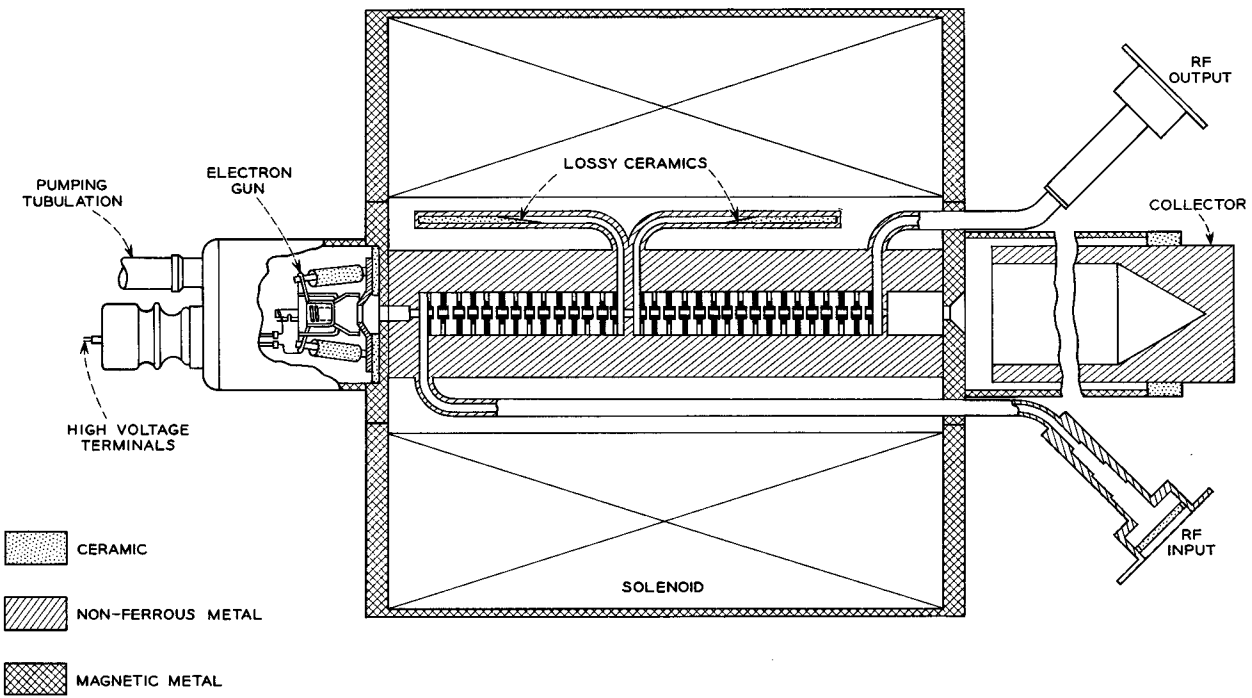


FIG. 10.2-7 The Bell Telephone Laboratories M4040 traveling-wave amplifier, a 2.6-kw, 6000-Mc tube.

in the beam induce currents into the second slow-wave structure section, and another 21 db of gain is produced. The power dissipated in the external sever termination results in an overall gain reduction of approximately 6 db, so that the net gain is 32 db. Without the beam present, the first and second sections of the slow-wave structure are completely isolated from each other. A slow-wave circuit which is terminated at some point near the middle for waves traveling in either direction is called a severed circuit.

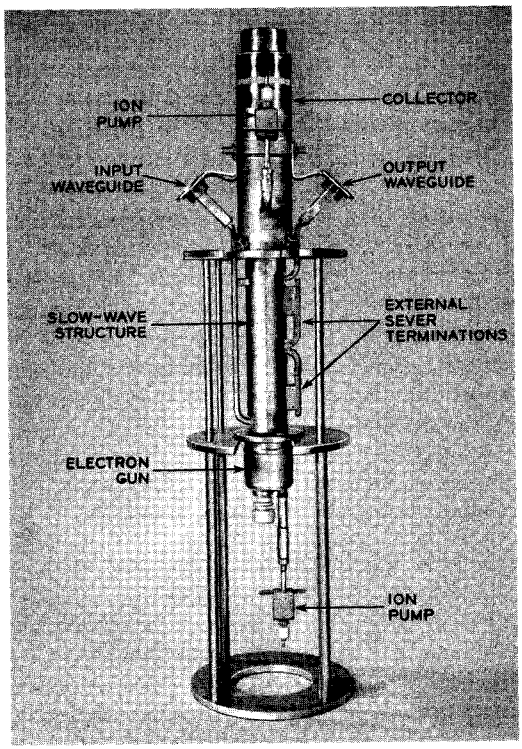


FIG. 10.2-8 The Bell Telephone Laboratories M4040. The overall height is 117 cm.

A severed circuit is necessary in a traveling-wave tube to prevent oscillations. Since it is impossible to match perfectly the input and output waveguides to the slow-wave structure over the entire operating frequency range, small rf reflections are invariably present at both ends of the structure. Without the sever, the wave reflected from the output connection travels back to the input with little attenuation and produces another small reflection. This provides a mechanism for positive feedback, and oscil-

lations result if the gain between the positions of these two reflections is large. Thus, severing the circuit keeps the gain per section low enough to prevent such oscillations.

The M4040 tube has the characteristics given in Table 10.2-1. It is operated in a solenoid which furnishes a uniform magnetic field of 730 oersteds.

TABLE 10.2-1. BTL M4040 OPERATING CHARACTERISTICS

| | |
|---|---|
| Center frequency, Mc | 6390 |
| Beam voltage, kv | 17 |
| Beam current, amps | 1.04 |
| Saturation power output, kw | 2.6 |
| Electronic efficiency at saturation, % | 15 |
| Small-signal gain, db | 32 |
| Small-signal bandwidth (1 db), Mc | 780 |

The tube plus solenoid weigh 230 pounds. Only $\frac{1}{2}$ per cent of the beam current is intercepted on the slow-wave circuit for small rf power levels; with output powers near saturation the circuit interception increases to about $3\frac{1}{2}$ per cent. The tube is operated with the collector at the same voltage as the slow-wave structure, so that approximately 14.5 to 17 kw of power is dissipated in the water-cooled collector, depending on the rf signal level. The length of the slow-wave circuit is 26 cm, and its inside diameter is 4.2 mm. The beam interaction impedance is 13 ohms. The electron gun is a convergent gun somewhat similar to that in Figure 4.5-1(a) Its perveance is $0.466 \times 10^{-6}$ amp/volts$^{3/2}$. It produces an electron beam of 2.3 mm diameter.

The ion pumps shown in the figure are electronic vacuum pumps which help to maintain an extremely high vacuum in the tube under all conditions of operation. The tube is constructed entirely of metal and ceramic. The slow-wave structure is made of copper because of the excellent electrical and thermal conductivity of this metal.

If we compare this tube with the VA-849 klystron amplifier, whose characteristics are given in Table 9.4-1, we note that the traveling-wave tube has much greater bandwidth and considerably less electronic efficiency. Thus, a choice between these two types in any particular application would depend largely upon the relative importance of bandwidth and electronic efficiency. It should be noted that the overall efficiency of each tube can be greater than the electronic efficiency if the collector voltage is lowered below the beam-interaction-space voltage.

## 10.3 Helix Slow-Wave Circuits

The most common slow-wave structure used in traveling-wave amplifiers is the helix. Helix-type, slow-wave circuits permit large bandwidth and

high gain per unit length. However, for rf output powers greater than 100 watts or so, a helix-type, slow-wave circuit would become excessively heated by beam interception and rf losses. Consequently, helix-type, slow-wave structures are used only at lower power levels.

In order to analyze the operation of the helix traveling-wave amplifier, we require information about the Brillouin diagram and the beam-coupling impedance. This information is obtainable by field analysis as in Chapter 8. However, the field analysis of the helix is a complicated mathematical problem; in fact, the exact solution for a helix of finite wire diameter has not been derived. The discussion presented here will be somewhat simplified, and we shall mention some of the more accurate results.

### (a) *The Brillouin Diagram for a Helix-Type, Slow-Wave Circuit*

The electric field lines surrounding a helix are shown in Figure 10.3-1. This field pattern moves to the right at a phase velocity corresponding to the fundamental space harmonic. Unlike the helix of Figure 8.7-2(a), this

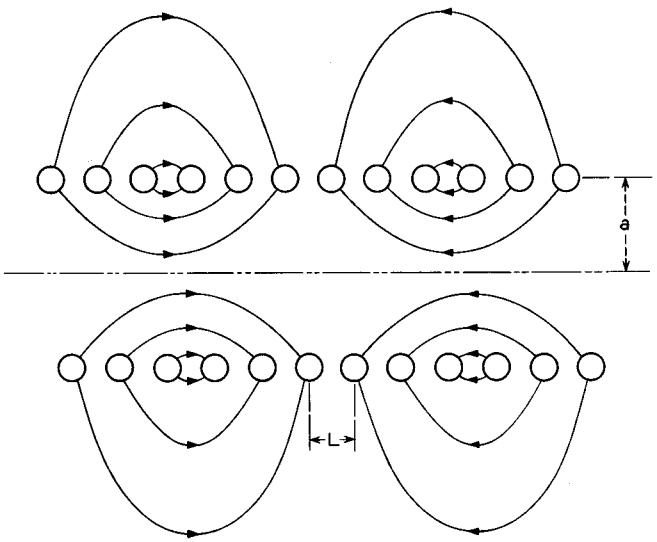


FIG. 10.3-1 The electric field lines surrounding a helix at a particular instant. The pattern travels at a phase velocity corresponding to the fundamental space harmonic.

helix does not have a surrounding metal tube. The helix in Figure 10.3-1 is shown unsupported. In practice, it would be supported by small dielectric rods or a surrounding dielectric cylinder, either of which would perturb the field pattern. However, we shall neglect this effect.

The period of the helix is called the pitch and is denoted by the symbol $L$. The mean radius of the helix is $a$. In addition, we define the pitch angle $\psi$ by the equation

$$\tan \psi = \frac{L}{2\pi a} \tag{10.3-1}$$

The wave equation for the $z$ component of electric field is obtained from Equations (10.2-8) and (10.2-9) as

$$\left[\frac{\partial^2}{\partial r^2} + \frac{1}{r}\frac{\partial}{\partial r} + \frac{1}{r^2}\frac{\partial^2}{\partial \theta^2} - \gamma_n{}^2\right] E_{zn} = 0 \tag{10.3-2}$$

In the case of the helix the field quantities are functions of $\theta$, the angular coordinate, since the boundary conditions vary with $\theta$. The space harmonics necessary to satisfy the helix boundary conditions are of the form[17]

$$E_{zn} = R_n(r)\epsilon^{\pm jn\theta}\epsilon^{-j\beta_n z} \tag{10.3-3}$$

where $R_n(r)$ is a function of only the radial coordinate for each space harmonic. The plus-or-minus choice for the $\theta$ dependence is dictated by the winding sense of the helix. Substituting this assumed solution into Equation (10.3-2), we obtain

$$\left[\frac{\partial^2}{\partial r^2} + \frac{1}{r}\frac{\partial}{\partial r} - \gamma_n{}^2 - \frac{n^2}{r^2}\right] R_n(r) = 0 \tag{10.3-4}$$

If we put $\gamma_n{}^2 = -\tau_n{}^2$, we recognize this as Bessel's Equation with the general solution

$$R_n(r) = b_n J_n(\tau_n r) + c_n H_n{}^{(1)}(\tau_n r) \tag{10.3-5}$$

where $J_n(\tau_n r)$ is the Bessel function of order $n$ and $H_n{}^{(1)}(\tau_n r)$ is the Hankel function of order $n$. Since $\tau_n = j\gamma_n$, the argument in the above functions is a purely imaginary number. Nevertheless, the values of the functions are either purely real or purely imaginary. The following modified Bessel functions are defined as to have purely real values:[18]

$$\begin{aligned} I_n(\gamma_n r) &= j^{-n} J_n(j\gamma_n r) \\ K_n(\gamma_n r) &= \frac{\pi}{2} j^{n+1} H_n{}^{(1)}(j\gamma_n r) \end{aligned} \tag{10.3-6}$$

$I_0(\gamma_0 r)$, $I_1(\gamma_1 r)$, $K_0(\gamma_0 r)$, and $K_1(\gamma_1 r)$ are plotted in Figure 10.3-2. The $I_n(\gamma_n r)$ functions go to infinity as $r$ goes to infinity. The $K_n(\gamma_n r)$ functions

[17]Reference 10c, pp. 46, 47.

[18]In order to avoid confusion with the beam interaction impedance, the Bessel function $K_n(\gamma_n r)$ will always be written showing its functional dependence. Tables of the modified Bessel functions are given in Reference 9.1, pp. 224–243.

go to infinity as $r$ goes to zero. Thus, $R_n(r)$ is given by $I_n(\gamma_n r)$ inside the helix and $K_n(\gamma_n r)$ outside the helix, in order that the fields remain finite everywhere. Each space harmonic has its maximum amplitude adjacent to

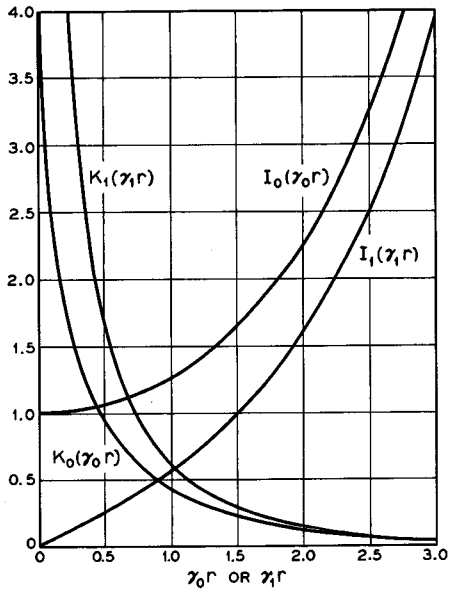


FIG. 10.3-2 Modified Bessel functions. $I_o(\gamma_o r)$ and $I_1(\gamma_1 r)$ apply to radial variations of fields within the helix, and $K_o(\gamma_o r)$ and $K_1(\gamma_1 r)$ apply to fields outside the helix.

the helix and decays radially away from the helix, both inside and outside the helix.

Thus we have the following expressions for the $z$ component of electric field. Inside the helix,

$$E_z = \sum_n B_n I_n(\gamma_n r) \epsilon^{\pm jn\theta} \epsilon^{-j\beta_n z} \tag{10.3-7}$$

Outside the helix,

$$E_z = \sum_n C_n K_n(\gamma_n r) \epsilon^{\pm jn\theta} \epsilon^{-j\beta_n z} \tag{10.3-8}$$

The amplitudes of the space harmonics are obtainable from the boundary conditions at the helix surface. This procedure has been carried out for a helix whose wires are thin tapes,[19] but not for round wires. After a rather

[19]References 10.7, 10.8.

lengthy, approximate analysis, one obtains expressions for the Brillouin diagram and beam interaction impedance. A similar analysis has been carried out for the sheath helix.[20] The sheath helix is a mathematical model consisting of a continuous, cylindrical sheath of currents, all flowing around the cylinder at the pitch angle. We shall not go through these analyses, but rather we shall cite some of the results.

First, it is found that the $\omega$-$\beta$ curve of the fundamental space harmonic of the tape helix is very nearly given by the $\omega$-$\beta$ curve of the fundamental

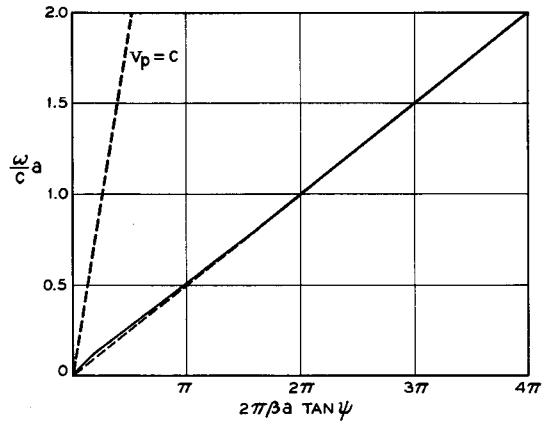


FIG. 10.3-3 $\omega$-$\beta$ curve for the fundamental mode of a sheath helix. The velocity-of-light line is shown for $\tan\psi = 0.125$.

mode of the sheath helix. The fundamental mode of the sheath helix is presented in Figure 10.3-3. It is approximately given by a line of constant slope from the origin corresponding to the phase velocity

$$v_p = \frac{\omega}{\beta} = c \tan\psi \tag{10.3-9}$$

This value of phase velocity corresponds approximately to that of a wave traveling around the cylinder at the pitch angle with the velocity of light, which is the value physical intuition would lead us to expect. (Note that $\beta$ here is equal to $2\pi/\lambda_z$, where $\lambda_z$ is the wavelength of the field pattern shown in Figure 10.3-1.) Let us approximate the actual $\omega$-$\beta$ curve of the sheath helix by the straight line with slope given by Equation (10.3-9). The wave may be made as slow as desired by choosing the pitch angle small enough.

[20]Reference 10a, Chapter 3.

Let us apply this sheath helix result to derive the Brillouin diagram of the tape helix. Using Equation (10.3-1) we note that the abscissa in Figure 10.3-3 may be written as $\beta L$ for the tape helix. Taking the straight line in Figure 10.3-3 as the fundamental space harmonic for the tape helix, we draw in additional space harmonics as in Section 8.7, obtaining Figure 10.3-4.

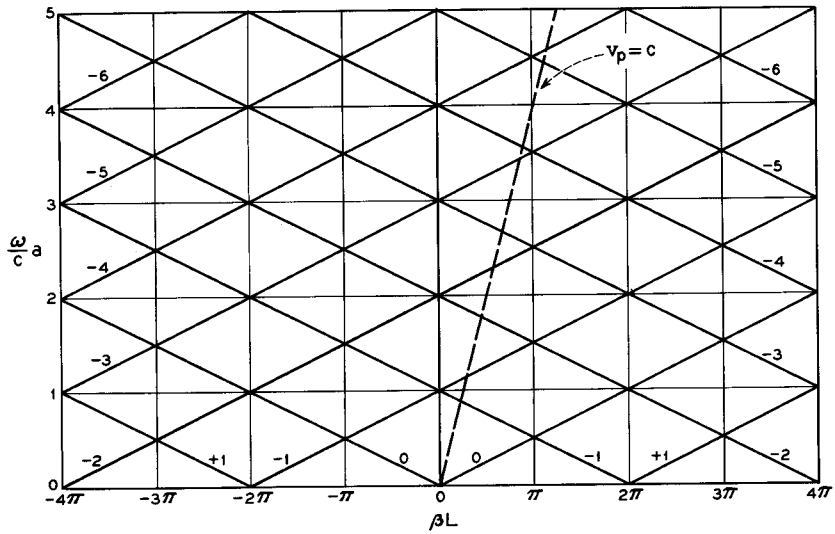


FIG. 10.3-4 Space harmonics corresponding to the straight-line approximation of the fundamental mode of a sheath helix. The branches are numbered as to the order of the space harmonic. The velocity-of-light line is shown for $\tan \psi = 0.125$.

In order to complete the Brillouin diagram for the tape helix we must include the so-called forbidden regions. The forbidden regions are regions in the Brillouin diagram for which electromagnetic energy is radiated away. In these regions the helix may be used as a helical antenna. Thus, the regions are forbidden in the sense that lossless propagation along the helix is not possible. The forbidden regions for the tape helix are shown shaded in Figure 10.3-5.

We can explain the existence of the forbidden region centered about $\beta L = 0$ in the following manner. Consider the form which the space-harmonic fields take exterior to the helix in this region. This region is characterized by the fact that all phase velocities are greater than the velocity of light. Thus, in this region,

$$\beta_n^2 < k^2 \tag{10.3-10}$$

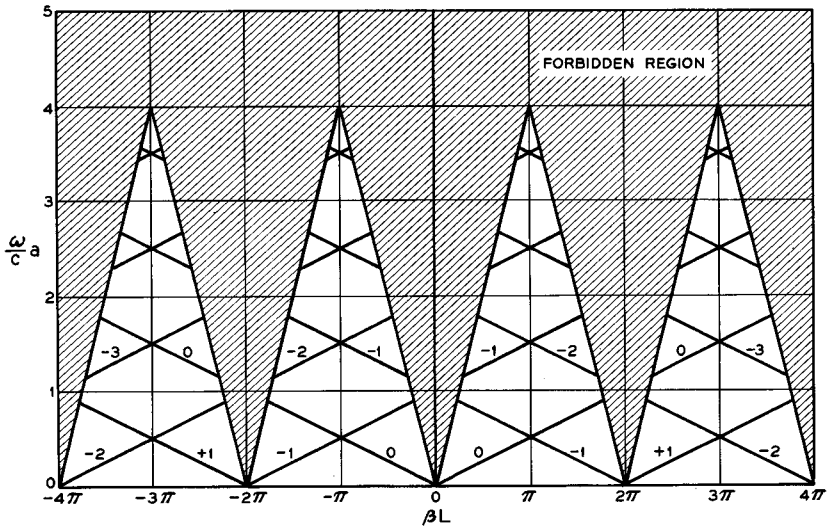


FIG. 10.3-5 Approximate Brillouin diagram for the tape helix, with $\tan\psi = 0.125$. In this approximation, changing the pitch angle changes only the lower extent of the forbidden regions. The branches are numbered as to the order of the space harmonic.

where $k = \omega/c$. This means that $\gamma_n = \sqrt{\beta_n^2 - k^2}$ is imaginary. If we put $\gamma_n = j\tau_n$, we obtain the following expression for $E_z$ external to the helix for the $n^{\text{th}}$ space harmonic,

$$E_{zn} = D_n H_n^{(1)}(-\tau_n r)\epsilon^{\pm jn\theta}\epsilon^{-j\beta_n z} \tag{10.3-11}$$

from Equations (10.3-6) and (10.3-8). For large radii the Hankel function has the asymptotic representation:[21]

$$H_{n\,r\to\infty}^{(1)}(-\tau_n r) = \sqrt{\frac{2}{\pi\tau_n r}}\epsilon^{-j(\tau_n r+\frac{n\pi}{2}+\frac{3\pi}{4})} \tag{10.3-12}$$

This radial variation corresponds to that of a cylindrical wave propagating radially to infinity. Thus for $\beta_n^2 < k^2$ the helix radiates energy, and by definition this is a forbidden region.

The other forbidden regions in Figure 10.3-5 are explained as follows. At any operating frequency all the space harmonics must exist in order that the boundary conditions be completely satisfied. Thus, if a portion of a space harmonic lies in the forbidden region described above, all the other space harmonics within the same frequency range are also forbidden.

These forbidden regions are responsible for the following important characteristics of the helix. First, the helix will not propagate above a

[21]Reference 10.2, p. 159.

certain frequency ($\omega a/c \cong 3.6$ for the conditions of Figure 10.3-5). Second, frequency stop bands are produced over ranges of frequencies approximately centered about $\omega a/c = 1, 2, 3$, etc.

### (*b*) *The Beam Interaction Impedance for a Helix-Type, Slow-Wave Circuit*

Next, we derive an approximate expression for the beam interaction impedance for the fundamental space harmonic of the helix. We do this by finding approximate expressions for the group velocity and stored energy per unit length. For the straight-line approximation to the Brillouin diagram, the group velocity is simply

$$v_g = v_p = \frac{\omega}{\beta_o} \tag{10.3-13}$$

We shall make use of the approximation $\gamma_o = \beta_o$, since $u_o \ll c$ for most helix tubes.

From a field plot as in Figure 10.3-1, we conclude that the $\theta$-component of electric field is small compared with the $r$ and $z$ components. Thus, we set $E_\theta = 0$. As a first approximation, we assume all the stored energy is in the fundamental space harmonic. For a thin tape helix the space-harmonic amplitudes must be the same at $r = a$ both inside and outside the helix, since the boundary conditions are identical. Thus, from Equations (10.3-7) and (10.3-8), we have

$$E_{zo} = B_o I_o(\gamma_o r)\epsilon^{-j\beta_o z} \tag{10.3-14}$$

inside the helix, and

$$E_{zo} = B_o \frac{I_o(\gamma_o a)}{K_o(\gamma_o a)} K_o(\gamma_o r)\epsilon^{-j\beta_o z} \tag{10.3-15}$$

outside the helix. Corresponding to these field components are the following radial components:

$$E_{ro} = jB_o \frac{\beta_o}{\gamma_o} I_1(\gamma_o r)\epsilon^{-j\beta_o z} \tag{10.3-16}$$

inside the helix and

$$E_{ro} = -jB_o \frac{\beta_o}{\gamma_o} \frac{I_o(\gamma_o a)}{K_o(\gamma_o a)} K_1(\gamma_o r)\epsilon^{-j\beta_o z} \tag{10.3-17}$$

outside the helix. The latter relationships may be verified using the divergence relation, Equation (6) of Appendix XII.

The average stored energy per unit length is equal to the peak electric

stored energy, given by[22]

$$W_{avg} = \frac{\varepsilon_o}{2}\int_0^\infty |E_{zo}|^2 + |E_{ro}|^2]2\pi r dr$$

$$= \pi\varepsilon_o |B_o|^2 \int_0^a [I_o^2(\gamma_o r) + I_1^2(\gamma_o r)]rdr$$

$$+ \pi\varepsilon_o |B_o|^2 \frac{I_o^2(\gamma_o a)}{K_o^2(\gamma_o a)} \int_a^\infty [K_o^2(\gamma_o r) + K_1^2(\gamma_o r)]rdr$$

$$= \frac{\pi a\varepsilon_o |B_o|^2}{\gamma_o} I_o^2(\gamma_o a)\left[\frac{1}{\gamma_o a I_o(\gamma_o a)K_o(\gamma_o a)}\right] \qquad (10.3\text{-}18)$$

The last term in the bracket is approximately equal to 2 over the useful range of the helix, as shown in Figure 10.3-6. Thus, we have the approximate expression

$$W_{avg} = \frac{2\pi a}{\gamma_o}\varepsilon_o |B_o|^2 I_o^2(\gamma_o a) \qquad (10.3\text{-}19)$$

Equation (10.1-19) may be written for the beam-coupling impedance as

$$K_o = \frac{\int |E_{zo}|^2 dS}{2\beta_o^2 S v_g W_{avg}} \qquad (10.3\text{-}20)$$

where the area integral is taken over the cross section of the beam. Introducing Equations (10.3-13), (10.3-14), and (10.3-19) we obtain

$$K_o = \frac{\int |B_o|^2 I_o^2(\gamma_o r)dS}{2S\frac{\beta_o}{\gamma_o}\omega 2\pi a\varepsilon_o |B_o|^2 I_o^2(\gamma_o a)}$$

$$= M_{2(0)}^2 \frac{30}{ka} \text{ ohms} \qquad (10.3\text{-}21)$$

where $M_{2(0)}^2$ is defined as in Equation (10.2-21). $M_{2(0)}^2$ varies between unity for a thin hollow beam grazing the helix and $1/I_o^2(\gamma_o a)$ for a thin solid beam on the axis. The expression given by Equation (10.3-21) for the impedance neglects the energy stored in the higher-order space harmonics. It can be shown[23] that the inclusion

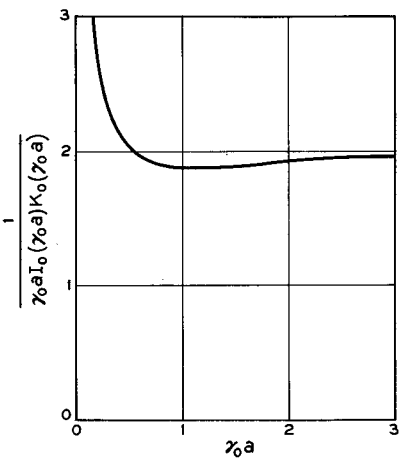


FIG. 10.3-6 Function of modified Bessel functions which is approximately equal to 2 over the useful range of the helix.

[22]Integrals of Bessel functions and useful identities are given in Reference 9.1, pp. 144–146. These relations may be written in terms of the modified Bessel functions using Equations (10.3-6).

[23]Reference 10.8.

of this additional energy reduces the impedance to approximately half that given by Equation (10.3-21). Thus, we have the useful approximate formula

$$K_o \cong M_{2(0)}{}^2 \frac{15}{ka} \text{ohms} \tag{10.3-22}$$

for the beam-coupling impedance of a tape helix where $k = \omega/c$. Although the foregoing relations are derived for a tape helix, they are also approximately valid for helices with round wires.

A typical helix tube may be designed for $ka = 0.1$ and $\gamma_o a = 1.5$. For a thin solid beam on the axis, Equation (10.3-22) gives a value of 55.3 ohms for $K_o$. This is considerably larger than values obtained with the high-power slow-wave structures discussed in the previous section. In comparing the Brillouin diagrams we see that the helix is capable of synchronism over much larger bandwidths than the high-power structures. Thus, the helix is superior in all respects except power handling capability.

### (c) *An Example of a Traveling-Wave Tube with a Helix-Type Slow-Wave Circuit*

Figure 10.3-7 shows the construction of the Western Electric 444A traveling-wave tube.[24] The slow-wave circuit consists of a molybdenum wire which is wound in a helix and glazed to three ceramic support rods. The helix assembly, consisting of the helix and support rods, slides inside a glass envelope of precise inside diameter. The electron gun is similar to that shown in Figure 4.5-1(a). An oxide-coated cathode is used.

Input and output connections to the helix are made by means of waveguides. The helix is "stretched" at each end and joined onto a cylindrical tubing which protrudes into the waveguide. This geometry provides a broadband rf match between the waveguide and the helix.

The magnetic circuit consists of two Alnico V magnets and two soft steel pole pieces. The circuit provides a nearly uniform axial magnetic focusing field of 600 oersteds. A number of permalloy "field straightener" discs are mounted perpendicular to the axis of the tube. Since these discs act as equipotential planes with respect to the magnetic field, they force the magnetic field to be axially symmetric with respect to the axis of the tube. The magnetic circuit is surrounded by an external magnetic shield (not shown in the figure) which reduces the leakage field outside the shield to a negligible value. The total weight of the magnetic circuit and shield is 85 pounds.

---

[24]Reference 10.9; the Bell Telephone Laboratories' 1789 tube is the prototype for the Western Electric 444A.

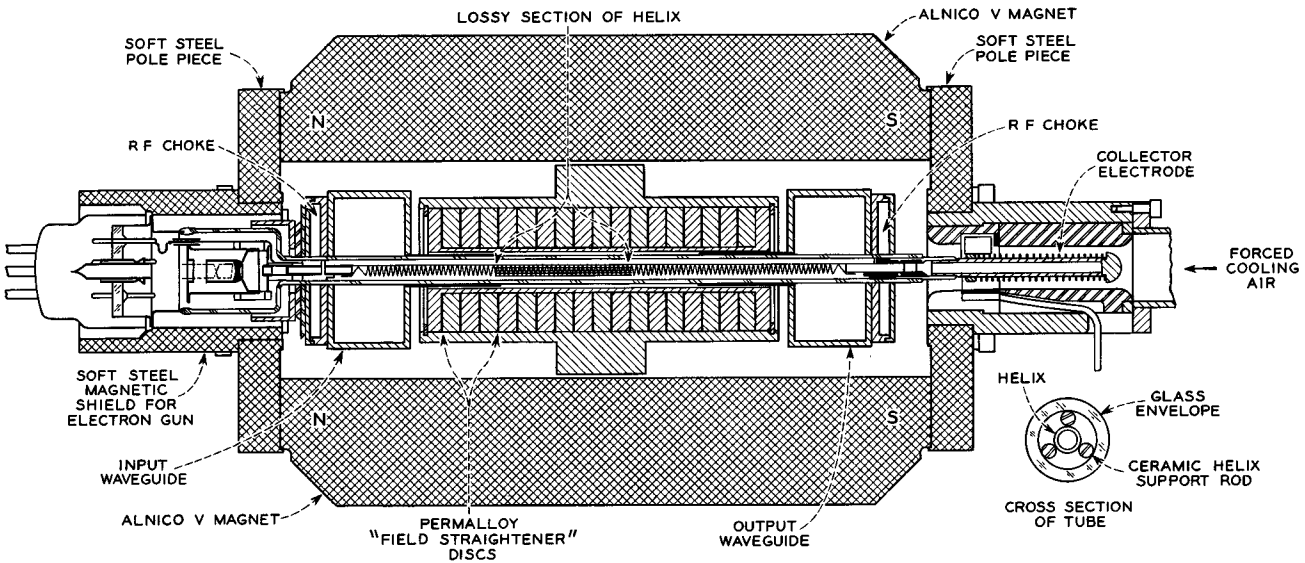


FIG. 10.3-7 The 444A traveling-wave tube and its magnetic focusing circuit. The input and output connections to the slow-wave circuit are made by means of waveguides. The axial magnetic focusing circuit is provided by two Alnico V magnets. (The polarity of the magnets does not matter provided both are magnetized in the same direction.) The thin permalloy "field straightener" discs are separated by thick nonmagnetic metal spacers. The tube can be removed from the magnetic circuit and replaced when it fails. The overall length of the tube is 31 cm.

Some additional facts about the tube are summarized in Table 10.3-1. The tube is used to provide rf amplification in a radio relay system over a band

TABLE 10.3-1. SOME FACTS PERTAINING TO THE 444A TRAVELING-WAVE TUBE

| | |
|---|---|
| *Helix* | |
| Mean diameter, $2a$, mm | 2.25 |
| Wire diameter, mm | 0.25 |
| Pitch, $L$, mm | 0.75 |
| Total turns | 187 |
| Length of helix, cm | 14 |
| *Beam* | |
| Voltage, volts | 2400 |
| Current, milliamps | 40 |
| Perveance, amps/volts$^{3/2}$ | $0.3 \times 10^{-6}$ |
| Beam power, watts | 96 |
| *RF Interaction* | |
| Signal frequency, Mc at midband | 6175 |
| $ka = \omega a/c$ | 0.148 |
| Axial wavelength, mm | 4.7* |
| Total number of wavelengths on helix | 30 |
| C | 0.058 |
| $QC$ | 0.29 |
| Operating power output, watts | 5 |
| Saturation power output, watts | 12 |
| Power gain at low signal levels, db | 32–36 |
| Power gain at 5 watts output, db | 31–35 |
| Electronic efficiency at saturation, % | 12.6 |

*6.3 turns of helix.

of frequencies 500 Mc wide and centered at 6175 Mc. Over this band of frequencies the power gain is flat to within 0.7 db. The 3-db bandwidth of the tube is approximately 2400 Mc and is limited primarily by the bandwidth of the transitions between the waveguide and helix.

Near the center of the helix, the helix and support rods are coated with carbon. This provides about 70 db of attenuation on the slow-wave circuit and prevents reflected waves from the output end of the circuit from causing oscillations. This forms a severed circuit as in Section 10.2(d).

The anode of the electron gun is operated at about 200 volts higher potential than the helix to prevent positive ions formed by the beam in the region of the helix from draining toward the cathode and bombarding the cathode. The air-cooled, copper collector is normally operated at only half the helix voltage, and hence half the voltage corresponding to the electron

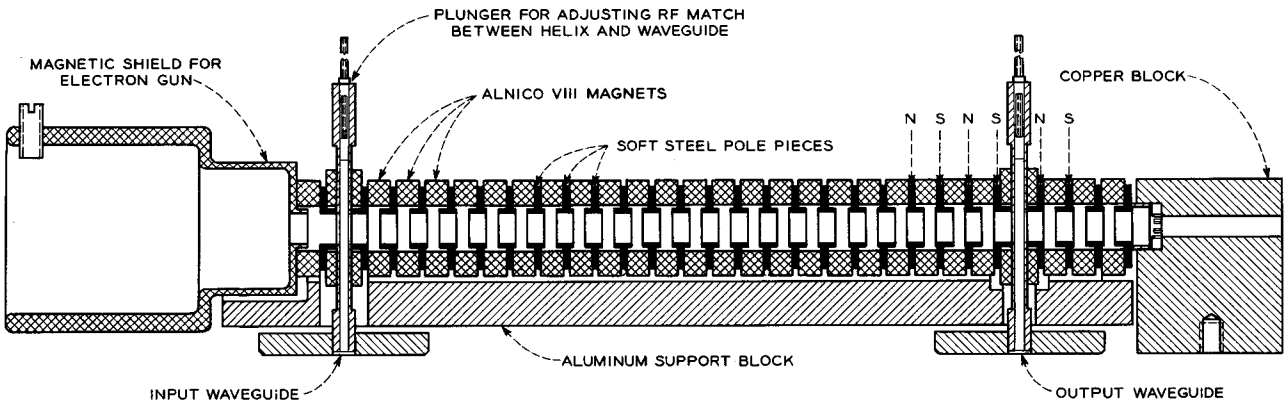


FIG. 10.3-8 A periodic permanent-magnetic (PPM) focusing system for a tube similar to the 444A. The overall length is 33 cm. The annular magnets are magnetized in the axial direction. They are stacked so that like poles of any two adjacent magnets face each other.

beam potential. Thus the overall efficiency of conversion of dc to rf power is twice the electronic efficiency.

At the time of writing, 67 per cent of an initial group of 212 444A tubes is surviving after two and one-half years of service in the radio relay system, and extrapolation of the data giving per cent survival vs. life indicates that half the tubes may survive between four and five years.

Figure 10.3-8 shows a cross-sectional view of a periodic magnetic focusing (PPM) circuit for a tube similar to the 444A. The circuit uses Alnico VIII magnets which give a peak axial magnetic field of 1000 oersteds. The leakage fields from this magnetic circuit are relatively small because of the short axial length of the individual magnets, and no external shielding is needed. The magnetic circuit is held together with an epoxy compound which is not shown in the figure. The total weight of the magnetic circuit is 8 pounds.[25] Waveguides of reduced height are used to couple rf power to the helix.

The broad bandwidths attainable with traveling-wave amplifiers make them ideally suited for broadband communication and radar systems. They are also useful as laboratory amplifiers. Bandwidths of 10 per cent in high-power tubes and 30 to 50 per cent in helix tubes are common. High gain tubes of 50 db or more are available; in this case, the circuit has more than one lossy section to prevent oscillations. Electronic efficiencies are good, but not as good as in the klystron amplifier. The positive feedback possible on the slow-wave circuit requires careful design to prevent oscillations, especially during the rise and fall times in pulsed operation, where the beam voltage is pulsed on and off.[26] High regulation and low ripple are required in the helix voltage supply to prevent undesirable phase-shift variations.

## *PROBLEMS*

10.1 The figure shows a typical connection of dc power supplies to a traveling-wave amplifier. Assume that the helix does not intercept any of the primary electron beam; neither does the anode of the electron gun.

(a) Which power supply provides the power that becomes useful rf power output?

(b) The bunched electron beam induces ac currents in the helix. If the helix were somewhat lossy, these currents would dissipate energy in the form of heat in the helix. Which power supply provides this energy?

---

[25]Other PPM stacks for similar tubes have weighed less than a pound, using platinum-cobalt magnets.

[26]As the voltage is increased toward the operating point, the electron velocity passes through points of synchronism with the phase velocity of the slow-wave structure where the impedance is very large (such as the point corresponding to $\beta_{-1}L = 2\pi$ in Figure 10.2-6). At such a point the danger of oscillation is greatest.

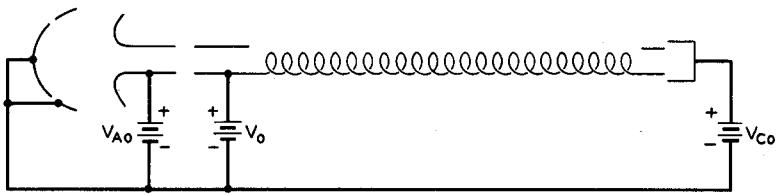


Problem 10.1

(c) If the beam current is $I_o$, what is the power supplied to the tube by the dc power supplies?
(d) The efficiency of the tube is defined as the ratio of maximum possible rf power output to the dc power input. Can the efficiency of the tube be raised by decreasing the potential $V_{C_o}$? Assume that the exchange of secondary electrons between the collector and helix can be neglected.
(e) If all the electrons are to be collected by the collector, how small can the voltage $V_{C_o}$ be made? Give only a qualitative answer.

10.2 The space-charge parameter $QC$ is the product of a dimensionless number $Q$ and $C$, the small-signal gain parameter. Show that $Q$ is independent of the beam current, as long as the beam current density is uniform over the beam cross section and the beam diameter is constant.

10.3 Using Figure 10.1-3 calculate the gain of a traveling-wave amplifier using the fundamental space harmonic under the following conditions:

$$f = 9 \text{ Gc}$$
$$K_o = 80 \text{ ohms}$$
$$QC = 0.50$$
$$I_o = 10 \text{ amps}$$
$$V_o = 25 \text{ kv}$$
$$d = 0.025$$
$$\beta_o = 725 \text{ radians/m}$$

Assume that a circuit sever reduces the over-all gain by 6 db and results in an effective interaction length $l$ of 7.62 cm. Neglect relativistic effects. *Ans.*: 33.3 db.

10.4 The traveling-wave amplifier theory developed in this chapter has assumed an infinite magnetic field so that transverse motion of the electrons is negligible. In a practical tube the magnetic field is finite. When a practical tube is operated with rf power output well below the maximum (or saturated) value, the percentage of the electron beam intercepted on the slow-wave structure is negligible. When the rf power input is increased so that the output power approaches saturation, the beam interception on the slow-wave structure often becomes 2 to 5 per cent of the total beam current. Explain qualitatively the reason for this increase.

10.5 Show that the apex of the triangle bounding the forbidden region for a helix is given by $\omega a/c = \pi a/L$.

10.6 Show that the beam-coupling impedance $K_o$ for a helix-type traveling-wave amplifier utilizing the fundamental space harmonic is given by

$$K_o = [I_o^2(\gamma_o b) - I_1^2(\gamma_o b)]K_o(0)$$

where $b$ is the radius of the electron beam which is centered on the axis and $K_o(0)$ is the impedance for an infinitesimally thin beam on the axis. The following integral will be useful:

$$\int_0^r rI_o^2(\gamma r)dr = \frac{r^2}{2}[I_o^2(\gamma r) - I_1^2(\gamma r)]$$

10.7 Using the result of the previous problem and Equation (10.3-22), calculate the impedance of a traveling-wave amplifier with $ka = 0.2$ and $\gamma_o a = 1.0$. The diameter of the electron beam is half the helix diameter.

10.8 When positive ions are present in an electron beam, the beam diameter tends to shrink, since the electron space-charge forces of repulsion are neutralized. When the collector voltage of a traveling-wave amplifier is depressed below that of the slow-wave structure, the ions are drained out of the beam into the collector and the beam diameter increases. What will be the effect on the gain of the amplifier when the collector voltage is depressed, assuming that the amount of electrons intercepted by the slow-wave structure is negligible?

10.9 A traveling-wave amplifier, with voltages applied as in Problem 10.1, operates under the conditions $b = QC = d = 0$, so that the gain is given by Equation (10.1-75). Amplitude modulation of the rf output may be obtained by varying the anode voltage $V_{Ao}$, with the other voltages and rf power input held constant.

(a) Show that the percentage change in rf power output is related to the percentage change in anode voltage by the expression:

$$\frac{dP_{\text{out}}}{P_{\text{out}}} = 5.45CN\frac{dV_{Ao}}{V_{Ao}}$$

(b) Which voltage should be varied to produce phase modulation on the rf output with a minimum of amplitude modulation?

10.10 The slow-wave structure of a traveling-wave amplifier is severed perfectly at a point sufficiently far from the input that only the growing wave is of importance. (Perfect severing implies that circuit waves from either direction are absorbed without reflection and also that the sever is so short that the beam convection current and velocity are unchanged before and after the sever.) Find the loss in over-all gain of the device in db due to the severing. Assume small $C$, and $b = QC = d = 0$. *Hint:* Rewrite and solve Equations (10.1-53) for the new initial values of electric field, velocity, and convection current just beyond the sever. The electric field is zero; the velocity and convection current are continuous from just before the sever. Find the ratio of the magnitudes of the growing wave $E_{zT1}$ just before and just after the sever. *Ans.*: 3.52db.

## *REFERENCES*

Three general references to the material of this chapter are:

10a. J. R. Pierce, *Traveling-Wave Tubes*, D. Van Nostrand Co., Inc., Princeton, N. J., 1950.

10b. A. H. W. Beck, *Space-Charge Waves and Slow Electromagnetic Waves*, Pergamon Press, Inc., New York, 1958.

10c. D. A. Watkins, *Topics in Electromagnetic Theory*, John Wiley and Sons, Inc., New York, 1958.

Other references covering specific items are:

10.1 J. A. Stratton, *Electromagnetic Theory*, McGraw-Hill Book Co., Inc., New York, pp. 131–132, 1941.

10.2 F. B. Hildebrand, *Advanced Calculus for Engineers*, Prentice-Hall, Inc., Englewood Cliffs, N. J., 1953.

10.3 W. H. Louisell, "Approximate Analytic Expressions for TWT Propagation Constants," *Trans. IRE* **ED-5**, 257–259, October, 1958.

10.4 C. K. Birdsall and G. R. Brewer, "Traveling-Wave-Tube Characteristics for Finite Values of C," *Trans. IRE* **ED-1**, pp. 1–11, August, 1954.

10.5 G. R. Brewer and C. K. Birdsall, "Traveling-Wave Tube Propagation Constants," *Trans. IRE* **ED-4**, pp. 140–144, April, 1957.

10.6 R. J. Collier, G. D. Helm, J. P. Laico, and K. M. Striny, "The Ground Station High-Power Traveling-Wave Tube," *Bell System Tech. J.* **42**, 1829–1861, July, 1963.

10.7 S. Sensiper, "Electromagnetic Wave Propagation on Helical Conductors," *Tech. Report No. 194*, MIT Research Lab. of Electronics, Cambridge, Mass., May, 1951.

10.8 P. K. Tien, "Traveling-Wave Tube Helix Impedance," *Proc. IRE* **41**, 1617–1623, November, 1953.

10.9 J. P. Laico, H. L. McDowell, and C. R. Moster, "Medium-Power Traveling-Wave Tube for 6000 Mc Radio Relay," *Bell System Tech. J.* **35**, 1285–1346, November, 1956.